Remote Sensing of Environment 186 (2016) 322–338

Contents lists available at ScienceDirect

Remote Sensing of Environment

journal homepage: www.elsevier.com/locate/rse

Linking seasonal foliar traits to VSWIR-TIR spectroscopy across California ecosystems

Susan K. Meerdink [a,*], Dar A. Roberts [a], Jennifer Y. King [a], Keely L. Roth [b], Philip E. Dennison [c], Cibele H. Amaral [d], Simon J. Hook [e]

[a] Department of Geography, University of California Santa Barbara, Santa Barbara, CA 93106-4060, United States
[b] Department of Land, Air, and Water Resources, University of California Davis, Davis, CA 95616-8627, United States
[c] Department of Geography, University of Utah, Salt Lake City, UT 84112, United States
[d] Department of Forest Engineering, Federal University of Viçosa, Avenida Purdue s/n, Campus Universitário, Viçosa, MG 36570-900, Brazil
[e] Jet Propulsion Laboratory, California Institute of Technology, Pasadena, CA 91109, United States

ARTICLE INFO

Article history:
Received 16 April 2015
Received in revised form 25 July 2016
Accepted 4 August 2016
Available online xxxx

Keywords:
Leaf traits
Visible Shortwave Infrared (VSWIR)
Thermal Infrared (TIR)
HyspIRI
AVIRIS
HyTES
Spectroscopy
Partial least squares regression

ABSTRACT

Vegetation traits provide critical information on ecosystem function that can be used to assess the effects of disturbance, land use, and climate change. Recent studies have demonstrated the use of spectroscopy to predict vegetation traits accurately and efficiently. To date, most spectroscopic studies have utilized data from the Visible Short Wave Infrared spectrum (VSWIR) or, occasionally, the Thermal Infrared spectrum (TIR), but not in combination. This study focuses on VSWIR and TIR synergy to evaluate the ability to predict leaf level cellulose, lignin, leaf mass per area (LMA), nitrogen, and water content across seasons. We used fresh leaves from sixteen common California shrub and tree species collected in the 2013 spring, summer, and fall seasons. The 284 samples exhibited a wide range of leaf traits as determined by standard analytical procedures: 4.2–27.3% for cellulose, 2.6–22.5% for lignin, 34.7–388.9 g/m^2 for LMA, 0.45–3.81% for nitrogen, and 20.2–76.9% for water content. For each leaf trait, partial least squares regression (PLSR) models were fit using different portions of the spectrum: VSWIR (0.35–2.5 μm), TIR (2.5–15.4 μm), and Full spectrum (0.35–15.4 μm). We also fit PLSR models using spectra resampled to simulate three airborne sensors: the Airborne Visible/Infrared Imaging Spectrometer (AVIRIS; 0.4–2.5 μm), the Hyperspectral Thermal Emission Spectrometer (HyTES; 7.5–12 μm), and the Hyperspectral InfraRed Imager (HyspIRI; 0.4–12 μm). The majority of best performing models used the Full spectrum, demonstrating the value of combining TIR and VSWIR spectra for leaf trait prediction. Sensor-simulated PLSR models created with the entire data set yielded validation R^2 and root mean square error of prediction (RMSEP) values as follows: $R^2 = 0.70$ and RMSEP = 13.1% for cellulose, $R^2 = 0.50$ and RMSEP = 17.7% for lignin, $R^2 = 0.56$ and RMSEP = 18.3% for LMA, $R^2 = 0.56$ and RMSEP = 18.1% for nitrogen, and $R^2 = 0.89$ and RMSEP = 5.7% for water content. General models successfully captured the variability among all seasons and leaf forms for cellulose and water content, while the other leaf traits were better modeled with season or leaf form-specific models. This study successfully captured the large seasonal and geographical variation in leaf traits across California's diverse ecosystems, supporting the possibility of using HyspIRI's imagery for global mapping efforts of these traits.

1. Introduction

Concerns over climate change, human-caused disturbances, and land-use effects on ecosystems have made it critical to quantify and characterize ecosystem functions, such as nutrient cycling, litter decomposition, and plant productivity (Ustin, 2013). Knowledge and understanding of these functions allow us to assess the health of an ecosystem. Plant traits play an important role in controlling these functions, which makes measurements of plant traits highly valuable (Ollinger et al., 2002; Smith et al., 2003; Atkin et al., 2015). However, traditional methods of collecting and processing extensive measurements of plant traits through time are expensive and time consuming. Using relationships derived between spectra (i.e., spectroscopy) and laboratory measured leaf traits can decrease processing time through faster analytical speed and minimal sample preparation (Lawler et al., 2006; Serbin et al., 2014). These relationships once derived using field plots or ground-based measurements can be used in conjunction with imaging spectroscopy to further increase spatial and temporal sampling (Asner et al., 2015).

To date, most spectroscopic studies have utilized the Visible Shortwave Infrared spectrum (VSWIR) to measure plant chemistry

* Corresponding author.
E-mail address: susan.meerdink@gmail.com (S.K. Meerdink).

http://dx.doi.org/10.1016/j.rse.2016.08.003
0034-4257/

and biophysical properties. Laboratory VSWIR spectroscopy began in the field of agriculture to measure forage quality (Shenk et al., 1979), but has since been extended to other vegetation traits from the leaf to canopy scale. At the leaf level, Serbin et al. (2014) determined seven spectroscopic models to predict leaf chemistry, morphology, and isotopic composition of temperate and boreal tree species with validation results ranging from R^2 of 0.60–0.97 and RMSEP of 4–16.2%. At the canopy level, Asner et al. (2011) used imaging spectroscopy at 61 sites located in humid tropical forests to predict 21 leaf trait properties with correlations ranging between an R^2 of 0.24–0.88 and RMSEP of 5.2–21.2%. More recently, Singh et al. (2015) developed seven canopy chemical and morphological prediction models across 51 images using Airborne Visible/Infrared Imaging Spectrometer (AVIRIS) with site-level $R^2 > 0.48$ and RMSEP < 15%. However, complications arise and model accuracy can decrease due to large portions of the VSWIR spectrum being obscured by water and pigment absorption features in fresh leaves, which hinder prediction capabilities for other leaf traits (Ribeiro da Luz and Crowley, 2010).

A smaller number of studies have used the Thermal Infrared (TIR) spectral measurements to describe plant characteristics. In general, the TIR wavelength region has not been widely adopted for vegetation studies due to the limited availability of TIR sensors and subtle features of plant spectra (Ribeiro da Luz and Crowley, 2007). However, there are exceptions, including Salisbury (1986) who was the first to show that spectral signatures varied among plant species in the 8–14 μm range. Elvidge (1988) followed by quantifying TIR reflectance features resulting from biochemical and biophysical traits of dry plant materials. More recently, Ullah et al. (2012) showed that plant species from the Netherlands have enough spectral diversity in the mid-infrared (MIR) from 2.5–6 μm and the TIR from 8 to 14 μm to support species discrimination. Another study, conducted by Fabre et al. (2011), found that leaf spectra in the 3–15 μm region were sensitive to variations in leaf water content. Research conducted by Ribeiro da Luz and Crowley (2007) identified spectral features in the TIR (8–14 μm) associated with cellulose, cutin, xylan, silica, and oleanolic acid. These studies support the use of information in the TIR region for quantifying leaf biochemical properties and improving species discrimination.

Integration of the VSWIR and TIR to cover a much larger range of wavelengths would enable researchers to utilize the strengths of each spectral region while minimizing limiting factors (Ribeiro da Luz and Crowley, 2007). However, little is known about the potential of combined VSWIR and TIR for ecological research due to a lack of studies in which both data types have been evaluated simultaneously. One of the few studies is by Ullah et al. (2014) who used the Full spectrum (0.39–14 μm) to successfully retrieve leaf water content from eleven different plant species. The main limiting factor for vegetation research using combined VSWIR and TIR data is the lack of sensors covering the full range of wavelengths. The proposed National Aeronautics and Space Administration (NASA) space-borne Hyperspectral InfraRed Imager (HyspIRI) mission would measure solar reflected and emitted radiance (Abrams and Hook, 2013; Green et al., 2013; Lee et al., 2015). The unique feature of HyspIRI is the inclusion of two instruments that measure wavelengths in the 0.38–12 μm range: an imaging spectrometer measuring the VSWIR wavelengths and a multi-spectral imager measuring several bands in the TIR (Lee et al., 2015). With these combined sensors, HyspIRI would provide combined VSWIR spectroscopy and broad band TIR data, enabling scientists to expand the wavelengths that can be used to estimate leaf traits and their relationships to ecosystem function. Still, the value of combined VSWIR-TIR data for estimating leaf traits is not fully understood, even at the leaf level.

The focus of this paper is to analyze synergies between the VSWIR and TIR prediction of leaf levels of cellulose, lignin, leaf mass per area (LMA), nitrogen, and water content across seasons. First we evaluate the capability of VSWIR and TIR spectra, individually and together, to predict lignin, cellulose, nitrogen, LMA, and water content. Secondly, we determine if these relationships can be extended to the reduced spectral resolution available in airborne and proposed spaceborne sensors, including the AVIRIS, the Hyperspectral Thermal Emission Spectrometer (HyTES), and the HyspIRI. Lastly, we test the development of a generalized and transportable model which captures the variability among seasons and leaf forms.

2. Methods

2.1. Study sites

We collected and analyzed plant samples from three different sites within California, United States: coastal Santa Barbara County, Sedgwick Reserve, and Sierra Nevada Mountains (Fig. 1). These study sites cover a large range in elevation (0–1400 m) with contrasting ecosystem characteristics (chaparral versus conifer forest) leading to a wide range of leaf traits and spectral values for analyses. The coastal Santa Barbara site is comprised of three sub-sites near the city of Santa Barbara, California and was designed to capture a cross section of the ecosystems present in coastal California (Fig. 1). These sub-sites were located at three elevations: 5 m, 515 m, and 1080 m. All three sub-sites are dominated by chaparral vegetation, a product of the region's Mediterranean climate which averages 38 cm of rain annually (Quinn and Keeley, 2006). Chaparral species form a nearly impenetrable thicket of shrubs with hard leaves and stiff twigs, which makes them well adapted for the hot, dry summers and unpredictable precipitation during the winter (Quinn and Keeley, 2006).

The Sedgwick Reserve site is located in the Santa Ynez Valley in Santa Barbara County, California (Fig. 1) and is the largest reserve within the University of California Natural Reserve System. With an annual precipitation of 38 cm, the three main vegetation communities are coastal sage scrub, oak woodland, and non-native grasses (Mahall et al., 2005). Our sampling locations within Sedgwick Reserve were located at elevations of 382 m and 400 m. The Sierra Nevada Mountains

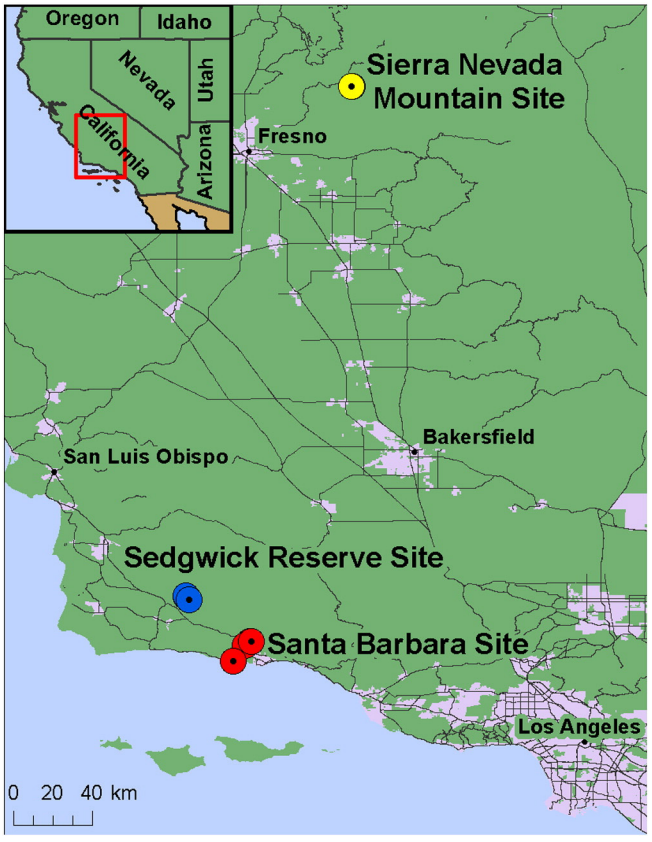

Fig. 1. Map showing locations of study sites.

site is located in the Sierra National Forest at an elevation of 1400 m (Fig. 1). At this elevation, the site is composed of mixed conifer forest with shrub-dominated rocky outcrops (Dahlgren et al., 1997). This site represents a wetter and cooler climate than our other study areas with an average precipitation of 101 cm per year (Dahlgren et al., 1997).

2.2. Leaf sample collection

We harvested a total of 284 samples from our sixteen study species, representing two leaf forms common to California (Table 1). Species, common name, leaf form, and date collected are shown in Table 1. Samples were collected from three individuals of each species, with sampling occurring once during each of the 2013 spring, summer, and fall seasons coinciding with the NASA HyspIRI airborne preparatory flights (Table 1). Three alternate BAPI individuals were chosen in the fall season at the Santa Barbara Coastal sub-site, due to the original plants being removed. In all other cases, leaves were sampled from the same individuals each season. Because individual leaves may live for several years, but may exhibit different trait values as they age, two age classes of leaves were collected: the current year's new growth and previous year's growth. New versus old growth was determined by leaf location on the branch along with other characteristics like leaf hardness, coloring, and size. Leaf collection was conducted for tree species using pole-clipping and for shrub species using pruning shears. Each sample was composed of multiple, randomly-selected leaves from the highest accessible part of the canopy. For shorter individuals, leaf samples were collected from the top of the canopy in full sun exposure, whereas samples from taller individuals received full sun part of the day. Each sample was subsequently divided into three subsamples for the following analyses: (1) Lignin, cellulose, and water content, (2) nitrogen and LMA, and (3) spectroscopy. The subsamples for spectroscopy and nitrogen analyses were placed in polyethylene bags with damp paper towels. These samples were kept cool in an ice chest (~10 °C), and a towel was used to prevent direct contact with ice. The subsamples for lignin, cellulose, and water content analyses were sealed tightly in high-density polyethylene (HDPE) bottles with polypropylene lids and stored at approximately 18–21 °C for <48 h until analysis.

2.3. Spectroscopy

Leaf spectral response was measured at the NASA Jet Propulsion Laboratory within 48 h of collection in order to preserve integrity of the samples. VSWIR spectral data were obtained using an Analytical Spectra Device (ASD) Field Spec 3 spectrometer, which measures the 0.3–2.5 μm range with an interpolated sampling interval of 1 nm (Analytical Spectra Devices, Inc., Boulder, CO, USA). The full width half maximum (FWHM) of this sensor is 3 nm at 0.7 μm, 10 nm at 1.4 μm, and 10 nm at 2.1 μm. The original sampling interval is 1.4 nm for the spectral region 350–1000 nm and 2 nm in the 1000–2500 nm region, which is interpolated to a finer sampling interval of 1 nm for a total of 2151 contiguous channels. Spectralon (Labsphere Inc., Durham, NH) was used as a calibrated reflectance standard to convert from raw radiance to relative reflectance. All samples were illuminated by a calibrated quartz halogen light source purchased from ASD, positioned at a 23° zenith angle and distance of 23 cm from the target. Spectra were collected using bare fiber (no foreoptic) with the fiber positioned at a 27° view zenith at a distance of 5 cm from the target, producing a 1.5 cm diameter field of view. This configuration results in bi-directional reflectance with a 50° phase angle. Each spectrum was calculated from the average of 30 scans. Spectral measurements for each sample included five spectra replicates per cluster of leaves followed by rotation of the target and a collection of another set of 5 replicates as allowed before reaching heat overload. When applicable, spectra were collected of the adaxial and abaxial leaf surfaces, but only reflectance from the adaxial leaf surfaces is reported in this paper. All spectra underwent quality assurance through visual assessment and spline correction for detector offset using ASD ViewSpec Pro splice correction (Analytical Spectra Devices, Inc., Boulder, CO, USA).

TIR spectral data were acquired using a Nicolet Model 4700 Interferometer Spectrometer fitted with a Labsphere gold coated integrating sphere (model RSA N1 700D) which measured emissivity from 2.5–15.4 μm with a sampling interval of 1 nm (Thermo Electron Corp., Madison, WI, USA) (Baldridge et al., 2009). The Nicolet 4700 uses a single EverGlo infrared light source which has a bulb temperature of 1140 °C to output a constant radiation. Dry air was sent into the external sphere to reduce the impact of moisture in the air on the spectra. Each spectrum was calculated from the average of 300 scans. Gold was used as a standard, and distilled water was used as a blank to check the accuracy of emissivity products. The Nicolet emissivity measurements were converted to reflectance by using Kirchhoff's Law (emissivity = 1 – reflectance), in order to match units with the VSWIR spectrum.

The sixteen species analyzed in this study were not able to fill the field of view with a single leaf for either the ASD or Nicolet. In order to fill the field of view, leaves were clustered while minimizing gap and overlap between leaves. For the ASD, all spectra were collected with a <5% reflective black background mat as a background to minimize background effects. For the Nicolet, leaves were placed on aluminum foil to minimize background effects that may be present from gaps. The Full spectrum (0.3–15.4 μm) was obtained by combining the VSWIR and TIR spectra (Fig. 2).

To generate reduced spectral resolution spectra, laboratory spectra were convolved to match the spectral resolutions of three systems: AVIRIS (VSWIR only), HyTES (TIR only), and HyspIRI (VSWIR and TIR). Laboratory spectra have different signal-to-noise ratios (SNR)

Table 1
Species sampled in the study.

Species	Common name	Abb.	Site	LF	Sampling dates
Abies concolor	White Fir	ABCO	Sierra Nevada	N	April 20, June 8, Nov. 2
Adenostoma fasciculatum	Chamise	ADFA	Santa Barbara	N	April 1, June 3, Oct. 13
Arctostaphylos glandulosa	Manzanita	ARGL	Santa Barbara	B	April 1, June 3, Oct. 13
Baccharis pilularis	Coyote Brush	BAPI	Santa Barbara	B	April 1, June 3, Oct. 13
Calocedrus decurrens	Incense Cedar	CADE	Sierra Nevada	N	April 20, June 8, Nov. 2
Ceanothus cuneatus	Buck-brush Ceanothus	CECU	Santa Barbara	B	April 1, June 3, Oct. 13
Ceanothus megacarpus	Big-pod Ceanothus	CEME	Santa Barbara	B	April 1, June 3, Oct. 13
Ceanothus spinosus	Green-bark Ceanothus	CESP	Santa Barbara	B	April 1, June 3, Oct. 13
Heteromeles arbutifolia	Toyon	HEAR	Santa Barbara	B	April 1, June 3, Oct. 13
Pinus lambertiana	Sugar Pine	PILA	Sierra Nevada	N	April 20, June 8, Nov. 2
Pinus ponderosa	Ponderosa Pine	PIPO	Sierra Nevada	N	April 20, June 8, Nov. 2
Quercus agrifolia	Coast Live Oak	QUAG	Sedgwick Reserve	B	April 21, June 9, Nov. 3
Quercus douglasii	Blue Oak	QUDO	Sedgwick Reserve	B	April 21, June 9, Nov. 3
Quercus lobata	Valley Oak	QULO	Sedgwick Reserve	B	April 21, June 9, Nov. 3
Salvia leucophylla	Purple Sage	SALE	Sedgwick Reserve	B	April 21, June 9, Nov. 3
Umbellularia californica	Bay Laurel	UMCA	Santa Barbara	B	April 1, June 3, Oct. 13

Note: LF (leaf form) is categorized by broadleaf (B) and needleleaf (N).

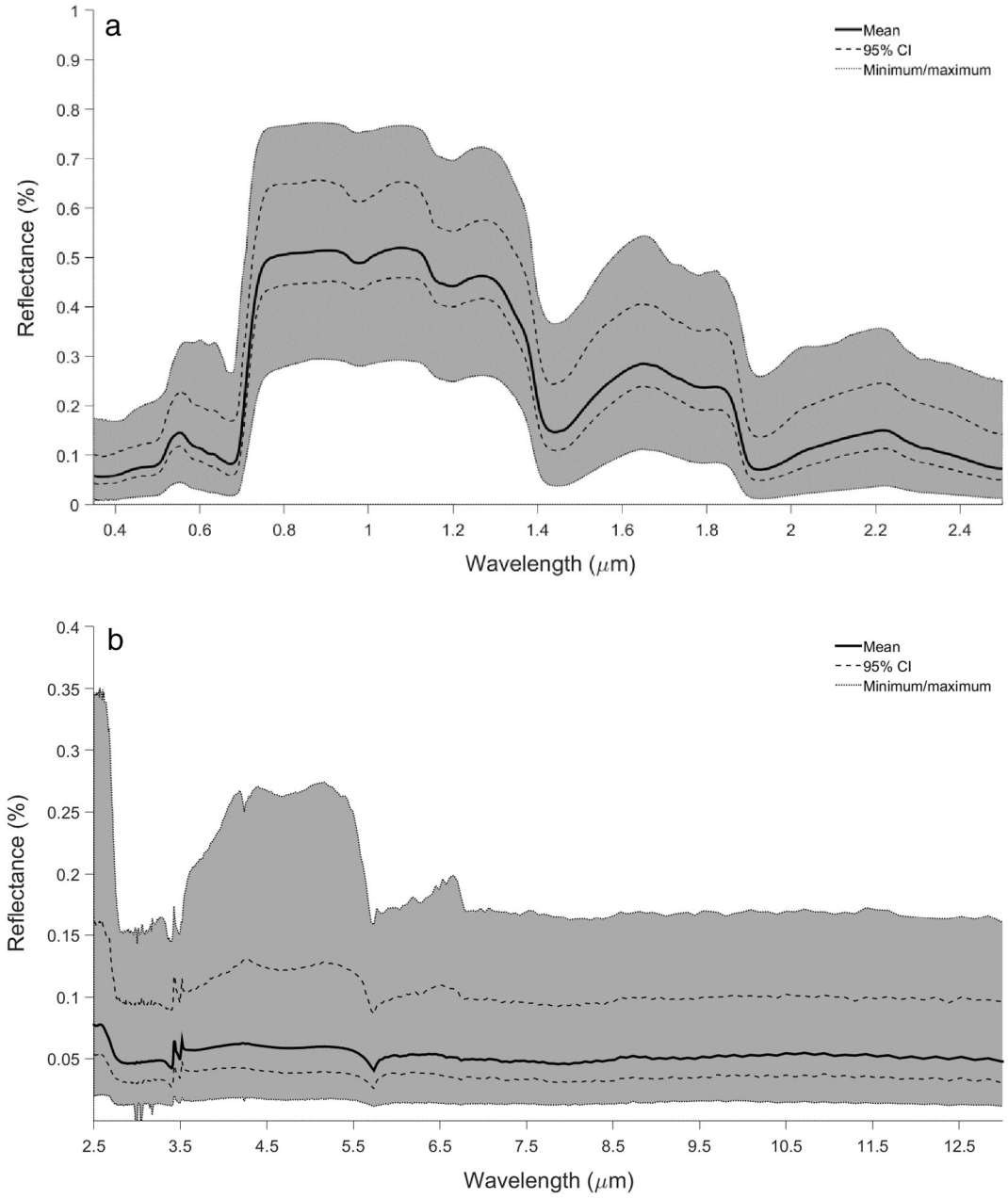

Fig. 2. The mean (bold, solid line), 95% confidence interval (dashed lines), minimum, and maximum (shaded area) spectral reflectance for (a) the VSWIR spectrum (0.35–2.5 μm) and (b) the TIR spectrum (2.5–13 μm) of all 284 samples.

compared to spectra from airborne and spaceborne spectrometers, and convolution to reduced spectral resolution greatly reduces noise. To better simulate spectra from AVIRIS, HyTES, and HyspIRI, artificial noise was added to the convolved spectra. To simulate AVIRIS data, VSWIR laboratory reflectance measurements were convolved using a Gaussian model with a 10 nm full-width half maximum (FWHM) and AVIRIS band center wavelengths spanning 400 to 2500 nm (Green et al., 1998). Adding noise to the simulated AVIRIS reflectance spectra required estimating radiance signal and noise. Band-by-band equivalent at-sensor radiance was modeled by MODTRAN using a range of surface reflectance values from 0 to 60% and typical sun-surface-sensor geometry and atmospheric variables (398 ppm for atmospheric carbon dioxide, 30° solar zenith angle, 1.2 cm column water vapor, 20 km sensor height, 0 km ground height, and 30 km visibility). Noise Equivalent delta Radiance (NEdL) was then calculated from modeled radiance based on the AVIRIS noise function described in Dennison et al. (2013). Dividing radiance by NEdL for each reflectance value and AVIRIS band allowed the generation of a SNR lookup table. Finally, noise was applied to the simulated AVIRIS spectra using a Gaussian random distribution, where one standard deviation was determined by the appropriate SNR value from the lookup table. To more closely simulate airborne measurements, the wavelengths falling within strong atmospheric water vapor absorption regions 1350 to 1450 nm and 1850 to 1975 nm were removed from AVIRIS simulated spectra (Gao and Goetz, 1995).

To simulate HyTES spectra, TIR laboratory based measurements were convolved using a Gaussian model with a 0.1 μm FWHM and HyTES band center wavelengths that ranged from 7.5 to 12 μm (Hook et al., 2013). To simulate HyTES sensor noise, we used the Noise Equivalent delta Temperature (NEdT) from HyTES to assign all temperature errors to the emissivity. The NEdT per band was provided by Johnson (2015). Using the NEdT, we calculated how much emissivity would have to deviate from a blackbody to generate the temperature errors. Using Kirchhoff's Law, the emissivity error was converted to reflectance.

Lastly, we applied the Gaussian random noise distribution to the reflectance spectrum. To determine the water vapor regions in this portion of the spectrum, H_2O transmittance was generated using MODTRAN for a sensor altitude of 1 km with a mid-latitude summer atmosphere (Berk et al., 2005). Wavelengths with <20% transmittance were removed.

The proposed HyspIRI sensor system was used to represent the Full spectrum (Lee et al., 2015). This sensor includes two instruments: a VSWIR imaging spectrometer measuring 0.38–2.5 μm and a TIR multispectral imager measuring from 3 to 12 μm (Green et al., 2013). The spectrum from 0.38–2.5 μm was modeled after the AVIRIS sensor. The spectrum from 3 to 12 μm was represented by eight bands located at: 3.98, 7.35, 8.2, 8.63, 9.07, 10.53, 11.33, and 12.05 μm. The TIR spectrum was convolved to these eight channels using a Gaussian model. To more accurately simulate the signal error of the proposed HyspIRI satellite, we used the same approach detailed for AVIRIS for the VSWIR portion of the spectrum, and the same procedure described for HyTES for the eight thermal bands instead using a NEdT of 0.1 K for each band (Johnson, 2015). Therefore, each HyspIRI spectrum was obtained by combining AVIRIS simulated spectra and the eight channel resampled TIR spectra.

2.4. Leaf traits

Lignin and cellulose were determined gravimetrically using a sequential acid digestion procedure with the Ankom Fiber Digestion Analyzer (ANKOM, Fairport, NY, USA). For this analysis, samples were oven-dried at 60 °C for at least 48 h and ground to pass through a 1 mm (20 mesh Wiley mill) screen. Subsamples of ~0.5 g were sealed in Ankom filter bags and subjected to sequential digestion to determine leaf fiber content (cellulose and lignin) and relative differences among species. There are known discrepancies between lignin determination methods because lignin is not easily quantified within various types of plant material (Hatfield and Fukushima, 2005). Currently there is not a widely-accepted standard lignin determination method, but the sequential digestion method is known to produce generally lower lignin concentrations overall (Hatfield and Fukushima, 2005). Thirty percent of samples were analyzed in duplicate for data quality assurance.

Percent leaf water content was calculated using the formula from Countryman and Dean (1979): leaf water content $= 100 * (Mw - Md)/Mw$, where Mw is the mass of the wet leaf and Md is the mass of the completely dried leaf. Mw was measured for each sample upon return to the laboratory, and Md was measured after samples were oven-dried at 60 °C for at least 48 h.

To obtain LMA, we covered a sheet of white 22.6 × 28 cm paper with leaf material and included a ruler for scale. The sheet was photographed using a Canon EOS Rebel T2i and Canon EFS 18–55 mm lens, which has ~18 megapixels. All leaf material was then transferred into a HDPE bottle with polypropylene lid. Samples were oven-dried at 70 °C for 72 h and then weighed. ImageJ software was used to calculate leaf area of photographed samples (Schneider et al., 2012) using particle recognition routines described by Richardson et al. (2001). LMA was then calculated as grams of dry mass per square meter of fresh leaf area.

After LMA analysis, samples were ground into a fine, homogeneous powder using a roller milling device and prepared for nitrogen analysis (Arnold and Schepers, 2004). Nitrogen content was obtained using a combustion method with the NA 1500 Series 2 Nitrogen and Carbon Analyzer (COSTECH Analytical, Valencia, CA, USA). Sample weights for analysis were ~8 mg. Thirty percent of samples were duplicated, and an acetanilide standard was run for every ten samples. Results are reported on a dry mass ash-included basis. One-way Analysis of Variance (ANOVA) was used to determine if leaf cellulose, lignin, LMA, nitrogen, and water content for each species varied significantly throughout all three seasons and among leaf forms (Table 2; Table A1).

2.5. Statistical methods

We modeled the relationships of spectra with cellulose, lignin, LMA, nitrogen, and water content using partial least squares regression (PLSR), implemented in the built-in MATLAB package (The Mathworks Inc., Natick, MA, USA). PLSR is similar to traditional regression models because a linear multivariate model is used to relate two data matrices, X and Y (Haaland and Thomas, 1988). PLSR is the traditional method in chemometrics and is widely used because of its sensitivity to a large number of highly correlated independent variables (Bolster et al., 1996; Doughty et al., 2011; Ferwerda et al., 2005; Martens et al., 1987; Wold and Sjostrom, 2001).

Leaf samples and spectra were used to build sets of PLSR models for estimating each leaf trait. In addition to a model covering all leaf forms and seasons, samples were sub-divided by season (spring, summer, and fall) and leaf form (broadleaf and needleleaf) to determine how predictive relationships might change based on these attributes. Therefore, six sets of PLSR model categories were created: general; spring; summer; fall; broadleaf and needleleaf. Within each model category, six sets of PLSR coefficients were derived using different input spectra: VSWIR, TIR, Full, AVIRIS, HyTES, and HyspIRI across 5 leaf traits for a total of 180 models.

To determine the number of factors to retain for each regression we used leave-one-out cross validation with all samples for each model category. This method reduces the possibility of over fitting the model with too many factors and produces a predicted residual error sum of squares (PRESS) statistic by total number of factors. The model with the minimum PRESS statistic is considered to have the optimum

Table 2
Foliar cellulose, lignin, LMA, nitrogen, and water content results for the sixteen target species averaged for all seasons and leaf ages.

Species	N	Cellulose (%)				Lignin (%)				LMA (g/m^2)				Nitrogen (%)				Water content (%)			
		Mean	Min	Max	SD	Mean	Min	Max	SD	Mean	Min	Max	SD	Mean	Min	Max	SD	Mean	Min	Max	SD
ABCO	18	13.4	10.7	16.9	1.7	10.8	8.6	13.0	1.3	258.8	171.3	361.1	45.3	0.91	0.74	1.20	0.12	53.5	46.5	60.8	4.3
ADFA	18	10.3	8.1	17.4	2.7	12.3	10.3	15.0	1.2	NaN	NaN	NaN	NaN	1.18	0.48	2.28	0.42	49.4	36.1	74.1	10.1
ARGL	18	6.8	5.5	8.1	0.7	10.9	8.0	14.6	1.8	224.7	120.6	336.1	74.6	0.72	0.45	1.07	0.16	47.0	40.2	61.7	6.7
BAPI	18	9.8	6.9	13.3	1.9	11.9	7.4	16.3	3.0	57.7	34.7	94.5	18.0	2.49	0.96	3.60	0.64	68.6	55.0	76.9	6.4
CADE	18	13.1	10.4	16.9	1.7	12.5	10.6	14.8	1.3	256.0	147.0	387.1	54.0	0.96	0.72	1.45	0.20	50.2	44.7	56.1	3.9
CECU	18	9.2	5.9	13.1	1.9	13.1	5.7	22.5	1.7	201.6	117.5	388.9	71.5	1.70	0.98	3.39	0.59	50.8	41.7	69.2	6.8
CEME	18	5.9	4.5	8.4	1.0	5.6	4.1	6.9	0.8	239.4	173.7	315.5	42.6	1.30	0.91	1.95	0.28	46.0	35.8	58.7	8.0
CESP	18	5.2	4.2	6.4	0.6	3.3	2.6	5.5	0.7	96.4	64.9	145.1	20.4	1.66	1.35	2.00	0.17	50.1	41.0	60.5	6.1
HEAR	18	10.4	8.5	14.0	1.6	10.2	7.0	12.0	1.1	161.7	84.6	220.5	40.7	1.31	0.78	2.02	0.29	53.5	47.4	66.6	5.0
PILA	18	18.2	16.0	20.9	1.5	10.1	8.7	11.9	1.0	237.5	168.4	336.9	52.7	0.90	0.69	1.40	0.17	52.2	44.2	58.8	4.5
PIPO	18	21.9	16.8	27.3	2.7	12.7	10.4	16.5	1.5	209.4	123.0	342.3	57.8	1.08	0.68	1.65	0.22	53.7	34.0	71.8	9.6
QUAG	18	18.7	14.9	21.6	1.5	12.1	10.0	14.0	1.3	220.6	98.0	314.7	52.8	1.30	0.79	2.19	0.29	43.6	28.8	61.5	5.8
QUDO	18	13.5	10.3	16.1	1.7	6.6	4.7	9.3	1.1	100.7	70.9	139.7	19.9	1.92	0.80	2.45	0.50	49.7	29.8	62.0	8.1
QULO	18	12.7	11.4	14.2	0.7	8.9	7.1	11.1	1.2	109.8	79.0	156.1	23.6	1.75	0.82	2.41	0.46	52.0	38.0	62.4	6.0
SALE	18	9.7	7.7	12.0	1.3	11.9	9.0	14.5	1.4	124.2	79.8	200.4	36.0	1.80	0.80	2.42	0.43	38.9	20.2	56.1	13.1
UMCA	18	10.0	7.5	11.5	1.2	11.8	10.4	15.6	1.4	101.9	46.7	147.8	28.8	2.16	1.06	3.81	0.78	54.1	46.9	75.3	9.1

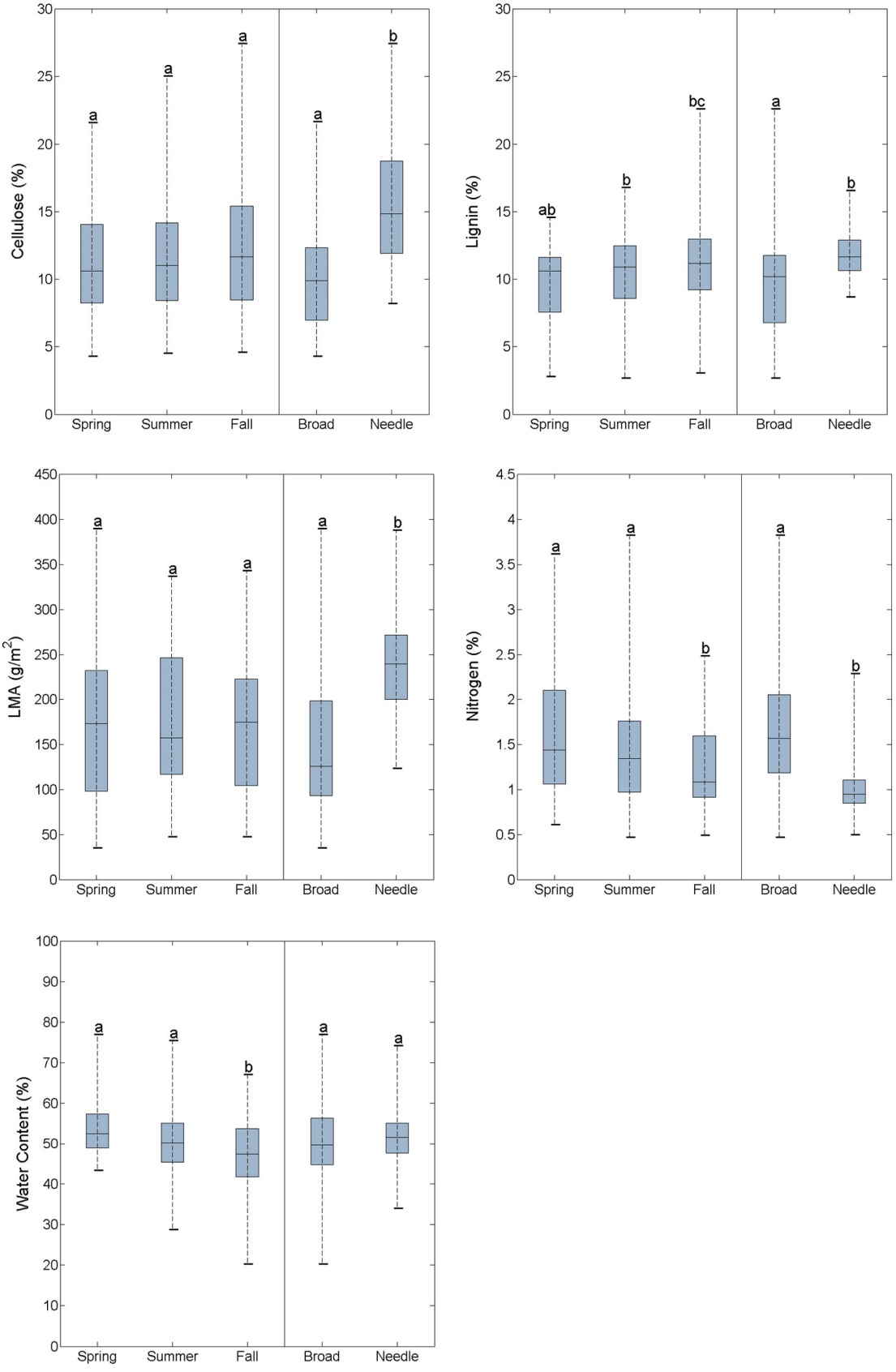

Fig. 3. Distribution of leaf traits by leaf form and season. The boxplots display the median for each trait by group (dark horizontal line), the interquartile range (boxes), and the data range (whiskers). Box plots labeled with different letters represent significant differences based on Tukey's honest significant difference criterion.

number of factors (Wold and Sjostrom, 2001). In many cases it is necessary to select a smaller number of factors than would be selected by minimizing the PRESS statistic to avoid over fitting the dataset (e.g. Martens et al., 1987; Serbin et al., 2012; Serbin et al., 2014; Singh et al., 2015). In this study, we selected the number of components where a local minimum of the PRESS statistic was present instead of a global minimum, and additional components did not result in a significantly improved PRESS statistic (as assessed with a *t*-test) (Serbin et al., 2014).

We randomly sampled our data into model calibration (80%) and external independent validation (20%) datasets. To ensure that both sets encompassed the range of measured leaf traits, samples were sorted and randomly selected within each quartile. Over 1000 iterations, model calibration data were randomly split into internal calibration (70%) and internal validation data (30%). Model development or internal calibration data were used to develop PLSR coefficients for leaf trait prediction and then applied to internal validation data for PLSR diagnostics. These 1000 model results were used to generate a mean PLSR model as well as means and distributions of all PLSR diagnostics. The coefficients from the 1000 model runs were then applied to the 20% of the data originally set aside for external validation. These data were never used in model development and are used to report model performance here. Model performance was measured using the coefficients of determination (R^2) and percent Root Mean Squared Error of Prediction (RMSEP) to report the accuracy of the models. To enable model comparison across leaf trait models, RMSEP was used because it is normalized by the percentage of the response data range (Feilhauer et al., 2010). Following our previously described experimental design, our analysis resulted in 36 models for each of the five leaf traits (180 models total). Results for each model, including the total number of samples, number of samples for validation, number of factors used in model, internal validation R^2 and RMSEP with standard deviations, and external validation R^2 and RMSEP are reported in Tables A2–A6. Internal calibration results are not shown. Here we discuss results for only the highest performing models based on external validation results from each of the six model categories.

3. Results

3.1. Seasonality and variability of leaf traits

The sixteen species chosen for this study exhibited a wide range in foliar cellulose, lignin, LMA, nitrogen, and water content values (Table 2). This range is important for accurate estimation with PLSR modeling and demonstrates both seasonal variations and differences across leaf forms.

Percent cellulose for all species ranged from 4.2–27.3%, with a mean of 11.8% and a standard deviation of 4.8%. Comparison between leaf forms showed significant differences in mean cellulose ($p < 0.0001$) (Fig. 3). When comparing seasonal samples, all seasons have similar mean cellulose content ($p < 0.484$) (Fig. 3). Six of the sixteen species had cellulose values that varied significantly by season ($p < 0.05$) (Table A1; Fig. A1). These seasonal differences corresponded with rapid leaf expansion that occurs within the first few months of the growing season and the resulting creation of cell wall material in new tissues (Mauffette and Oechel, 1989).

The range of lignin content for all species varied from 2.6–22.5% and had a mean of 10.3% with a standard deviation of 3.4%. Mean lignin content was lower for needleleaf samples and broadleaf had a much wider variation ($p < 0.0001$) (Fig. 3). Across seasons, lignin increased in the fall ($p < 0.035$) (Fig. 3). Eight of sixteen species varied significantly by season ($p < 0.05$) (Table A1; Fig. A2). The increased lignin content in sampled leaves from April to November can be explained by the fact that lignin concentration increases as leaves become rigid and woody (i.e. lignify) with age (Martin and Aber, 1997).

LMA had a range of values from 34.7–388.9 g/m^2 with a mean and standard deviation of 173.5 and 80.4 g/m^2, respectively. LMA differed greatly between leaf forms, with needleleaf having the largest values and broadleaf the smallest ($p < 0.0001$) (Fig. 3). This is consistent with literature that demonstrates that LMA varies widely between leaf forms (Poorter et al., 2009). There were no significant differences among seasons for LMA ($p < 0.763$). However, at the species level, there were differences among seasonal LMA for six of the sixteen species ($p < 0.05$) (Table A1; Fig. A3). This pattern can be explained by new growth that occurs in either the spring or summer season depending on species' phenology (Jurik, 1986).

Nitrogen content exhibited a range of values from 0.45–3.81% with a mean of 1.4% and standard deviation of 0.6%. Differences in mean nitrogen content between leaf forms was statistically significant, with broadleaf samples having a larger variation and higher nitrogen content compared to needleleaf samples ($p < 0.0001$) (Fig. 3). Seasonal differences in mean nitrogen were also statistically significant, with spring having the highest content ($p < 0.001$) (Fig. 3). Seven of the sixteen species exhibited this same pattern ($p < 0.05$) (Table A1; Fig. A4). Nitrogen content was higher in new leaves compared to mature foliage, which corresponded to the timing of new growth (either spring or summer) for these seven species (Mauffette and Oechel, 1989).

Water content varied greatly with values from 20.2–76.9%, and a mean and standard deviation of 51.0% and 9.3%, respectively. Water content was not significantly different between the two leaf forms ($p < 0.329$) (Fig. 3). Seasonal variation in water content was strong with decreasing values from the spring to fall season ($p < 0.0001$) (Fig. 3). This was especially evident for individual species, where thirteen of the sixteen species showed significant seasonal changes in water content ($p < 0.05$) (Table A1; Fig. A5). Of these thirteen species, eleven species collected from the Sedgwick Reserve and Santa Barbara sites had lower water content in the fall season, which corresponds to leaf senescence (Ustin et al., 1998). The other two species were collected in the Sierra Nevada Mountain site and had the highest water content in the fall.

3.2. Laboratory spectra models

For each leaf trait, we compared the highest performing PLSR models created using laboratory measured VSWIR, TIR, and Full range spectra for each of the six model categories (general, leaf form-specific, season-specific). The best models for all leaf traits created from laboratory spectra had RMSEP of 5.6–33.5% and R^2 of 0.00–0.91 (Table 3). The highest performing models, based on lowest average RMSEP, were water content, followed by cellulose, lignin, LMA, and nitrogen which had the highest RMSEP. Water content models had R^2 values from 0.81–0.91 and RMSEP values from 5.6–13.6% (Table 3; Table A6). Cellulose prediction models performed well with R^2 values of 0.68–0.87 and RMSEP values of 11.6–17.6% (Table 3; Table A2). Models of lignin had R^2 values of 0.39–0.69 and RMSEP values of 14.4–23.1% (Table 3; Table A3). LMA had the largest variation compared to other leaf traits in laboratory spectra model results. Models ranged from R^2 of 0.06–0.80 and 13.6–33.5% RMSEP (Table 3; Table A4). Nitrogen prediction using laboratory spectra had the lowest average performance out of all five leaf traits. Prediction of nitrogen content had R^2 values ranging from 0.01–0.57 and RMSEP of 17.9–30.8% (Table 3; Table A5).

Out of the best 30 laboratory spectra models across all five leaf traits, fourteen models used the Full spectral range, twelve used the VSWIR, and only four used the TIR spectrum. The majority of best performing models for lignin and LMA used the Full spectrum. On the other hand, nitrogen models used the Full, VSWIR, and TIR spectra equally. The best cellulose and water content models used both VSWIR and Full spectrum equally. In summary, the TIR laboratory spectra did not yield a large number of best performing models while the combined VSWIR-TIR range ultimately yielded the greatest number of best performing models with a slight improvement over using VSWIR alone.

For leaf form-specific models, there was wide variation in model performance between broadleaf and needleleaf models (Table 3). In general, the broadleaf models had a higher R^2 and lower RMSEP compared to needleleaf for all leaf traits except for cellulose. For cellulose, lignin, and water content the difference in broadleaf versus needleleaf prediction performance was minimal. Nitrogen had a 9.9% difference between needleleaf and broadleaf models. However for LMA the difference was greater (19.3% difference) with the broadleaf having a higher model performance. Ultimately, model performances for leaf form-specific models were different depending on the leaf trait analyzed; in general broadleaf models outperformed needleleaf models.

Seasonal model performance was also highly variable, but less so compared to leaf form-specific models (Table 3). Across all leaf traits, the summer models generally had the highest performance with average RMSEP of 15.9%, while spring had similar performance with an average RMSEP of 16.8%. Fall models had the poorest performance with an average RMSEP of 19.4%. For lignin and cellulose the highest performing models were the spring season, while for LMA, nitrogen, and water content the highest performing models were the summer season. For each leaf trait the RMSEP only varied between 4.7 and 8.7% among spring, summer, and fall models, while between broadleaf and needleleaf models RMSEP varied between 1.5 and 19.3%.

The general models for all five leaf traits had $R^2 = 0.55–0.91$ and RMSEP = 5.62–18.31% (Fig. 4). The water content general model had the highest performance using the Full spectrum ($R^2 = 0.91$ and RMSEP = 5.62%) and used the fewest number of factors ($h = 7$) compared to the other four leaf traits. The cellulose general model showed the next best performance with $R^2 = 0.76$ and RMSEP = 11.59%. General models for lignin, LMA, and nitrogen had similar model performance with $R^2 = 0.55$, 0.57, 0.57 and RMSEP = 17.2, 18.31, 17.89%, respectively. For cellulose, nitrogen, and water content, the general PLSR model yielded the highest R^2 and lowest RMSEP compared to leaf form or season-specific models. However for lignin and LMA, the general model did not outperform leaf form or season-specific models. For lignin, the general model was very similar to average model performance with the spring and summer seasonal models outperforming the general model. For LMA, the general model yielded the second lowest performing model with only the needleleaf performing worse.

We used the standardized PLSR coefficients to identify the regions of the spectrum that were significant to the general model calibrations (Fig. 5). For cellulose, lignin, LMA, and water content, the coefficients with largest magnitude lie in the VSWIR region of the spectrum (Table 4). As well, for all leaf traits several influential coefficients were found in the 2.5–4 μm range. Generally low coefficient magnitudes were found in the TIR region.

3.3. Sensor simulated spectra models

Reduced spectral resolution models (simulating existing and proposed sensors) had decreased model performance compared to the models derived from laboratory spectra. Models using sensor-simulated spectra had RMSEP values that ranged from 5.8–30.4%, and R^2 values that ranged from 0.22–0.91 (Table 5). Average model performance by leaf trait ranked from highest to lowest as follows: water content, cellulose, lignin, LMA, and nitrogen. Water content prediction models had R^2 values of 0.71–0.89 and RMSEP values from 5.7–16.8% (Table 5; Table A6). Cellulose models followed with R^2 ranging from 0.52–0.91 and RMSEP from 10.3–21.4% (Table 5; Table A2). Lignin prediction models had R^2 values ranging from 0.42–0.67 and RMSEP of 14.6–23.2% (Table 5; Table A3). LMA models had R^2 values from 0.37–0.82 and RMSEP values from 14.7–26.4% (Table 5; Table A4). Nitrogen model performance varied more than other leaf traits with R^2 values ranging from 0.22–0.82 and RMSEP values from 17.4–30.4% (Table 5; Table A5).

Out of the best 30 sensor-simulated spectra models across all five leaf traits, thirteen models used HyspIRI, twelve used AVIRIS, and only five used HyTES. For cellulose, lignin, and LMA, the HyspIRI spectral

Table 3
Best performing models using laboratory spectra for each leaf trait and model category. Performance was determined using external validation results. N is total number of samples, N_{val} is the number of samples set aside to calculate validation statistics, and h is the number of factors used to build PLSR models.

	Model					Internal validation		External validation	
	Category	Spectrum	N	N_{val}	h	R^2 (S.D.)	RMSEP (S.D.)	R^2	RMSEP
Cellulose	General	Full	284	57	14	0.65 (0.06)	13.45 (1.83)	0.76	11.59
	Broadleaf	VSWIR	194	37	11	0.57 (0.09)	15.79 (2.65)	0.70	14.72
	Needleleaf	VSWIR	90	17	14	0.66 (0.15)	17.34 (4.47)	0.81	12.67
	Spring	Full	96	19	13	0.63 (0.10)	18.09 (3.65)	0.87	12.09
	Summer	VSWIR	95	18	12	0.64 (0.12)	15.93 (3.45)	0.69	17.56
	Fall	Full	93	18	12	0.59 (0.10)	17.13 (3.93)	0.68	16.93
Lignin	General	Full	284	56	10	0.49 (0.07)	14.41 (2.02)	0.55	17.20
	Broadleaf	Full	194	39	14	0.54 (0.08)	17.75 (3.08)	0.54	17.64
	Needleleaf	VSWIR	90	18	14	0.36 (0.15)	22.41 (4.56)	0.39	21.45
	Spring	Full	96	20	11	0.69 (0.08)	13.59 (2.16)	0.69	14.41
	Summer	TIR	95	18	10	0.56 (0.11)	17.91 (4.96)	0.58	16.59
	Fall	VSWIR	93	18	8	0.32 (0.14)	24.17 (7.79)	0.46	23.14
LMA	General	Full	265	53	14	0.67 (0.05)	13.50 (1.58)	0.57	18.31
	Broadleaf	Full	195	39	13	0.62 (0.07)	16.60 (2.36)	0.73	14.15
	Needleleaf	TIR	70	14	10	0.05 (0.05)	29.11 (9.94)	0.06	33.48
	Spring	VSWIR	90	17	14	0.48 (0.14)	21.53 (5.32)	0.68	18.26
	Summer	Full	90	16	10	0.67 (0.09)	17.44 (3.45)	0.80	13.58
	Fall	VSWIR	85	17	12	0.65 (0.11)	17.87 (3.63)	0.77	16.00
Nitrogen	General	TIR	284	56	10	0.29 (0.09)	24.35 (3.57)	0.57	17.89
	Broadleaf	VSWIR	195	36	9	0.44 (0.10)	13.96 (2.91)	0.47	20.97
	Needleleaf	VSWIR	89	17	8	0.48 (0.22)	18.13 (5.03)	0.01	30.83
	Spring	TIR	96	18	11	0.50 (0.18)	23.45 (6.92)	0.41	25.46
	Summer	Full	96	18	11	0.45 (0.16)	28.85 (6.85)	0.41	23.35
	Fall	Full	92	18	10	0.35 (0.16)	28.00 (6.46)	0.37	28.70
Water content	General	Full	284	53	7	0.69 (0.09)	9.85 (1.57)	0.91	5.62
	Broadleaf	VSWIR	194	37	6	0.71 (0.09)	11.01 (1.99)	0.83	7.45
	Needleleaf	Full	90	18	8	0.69 (0.10)	11.46 (2.17)	0.87	8.91
	Spring	Full	96	18	12	0.74 (0.11)	14.71 (4.70)	0.81	13.57
	Summer	VSWIR	95	16	5	0.42 (0.19)	16.55 (3.69)	0.84	8.63
	Fall	VSWIR	93	18	5	0.78 (0.09)	11.27 (2.78)	0.81	12.35

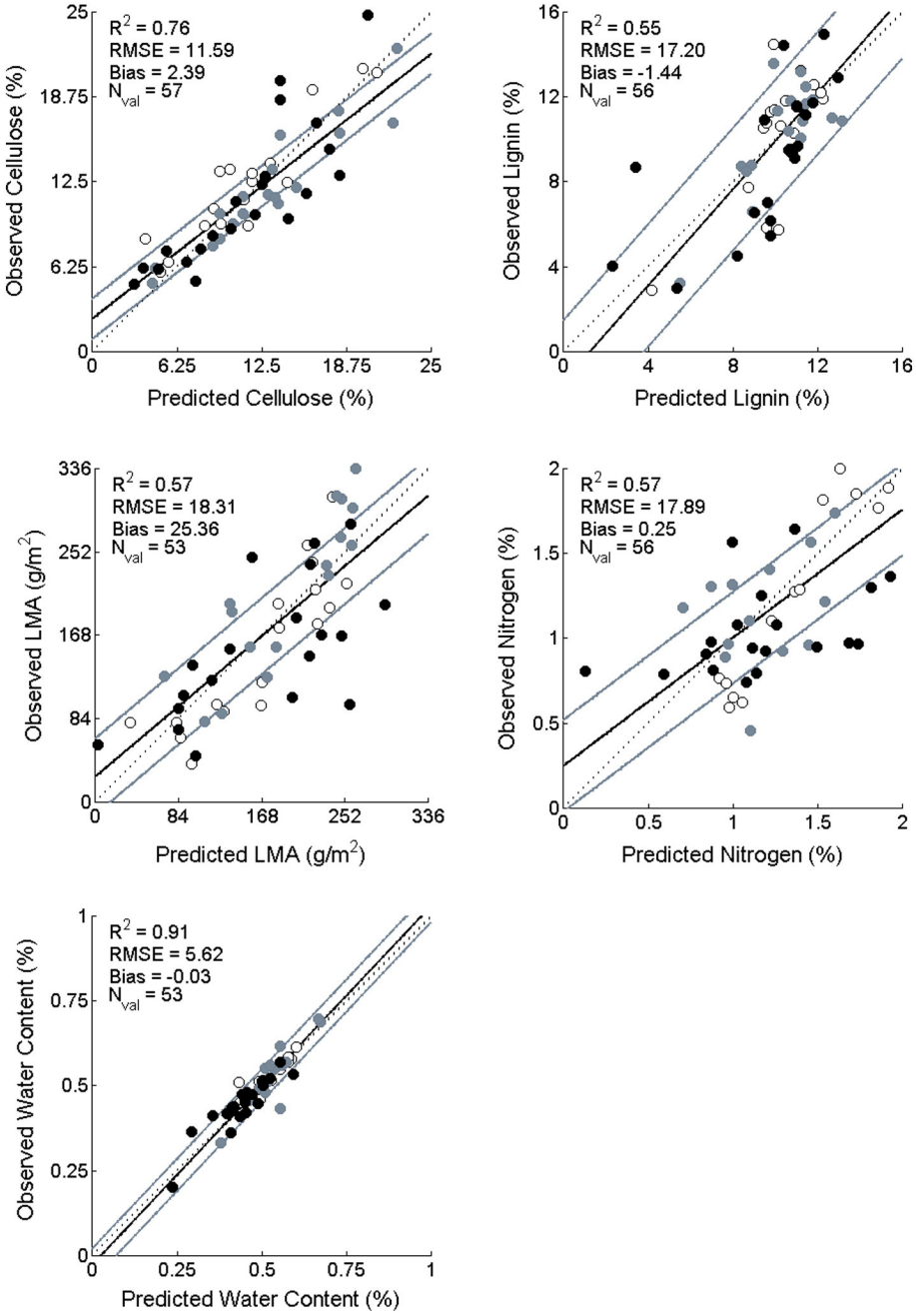

Fig. 4. Independent validation results for the best performing laboratory general PLSR models. Dark line denotes regression line, light gray lines show the 95% confidence intervals of the models, and dashed line shows the 1:1 line. Black symbols denote spring season samples, gray symbols denote summer, and white symbols denote fall.

range yielded the highest number of best performing models compared to AVIRIS or HyTES. For nitrogen and water content, the AVIRIS spectrum yielded the highest number of best performing models. Both LMA and nitrogen had two best models using the HyTES spectrum. At the reduced spectral resolution in available and proposed sensors, the HyspIRI spectrum has a slight majority of best performing models over AVIRIS or HyTES for all five leaf traits (Table 5).

Leaf form-specific models showed that the broadleaf leaf form had the highest model performance for all leaf traits except lignin. For cellulose and lignin, the difference in broadleaf versus needleleaf prediction performance was minimal, but for LMA, there was an 11.7% difference between needleleaf and broadleaf model performance, with broadleaf leaf form having a higher model performance.

According to average RMSEP values, spring seasonal models performed best (RMSEP = 15.2%) followed by summer models (RMSEP 18.3%) and followed by fall seasonal models (RMSEP = 21.4%). The spring season had the best performance for cellulose, lignin and nitrogen, while those from the summer season had the best performance for LMA and water content. For water content prediction among seasons, the model performance varied the least with only a 6.1% RMSEP total difference. On the opposite end, nitrogen seasonal models had a 13.0% RMSEP difference total. Seasonal models varied more for broadleaf versus needleleaf models.

The general models for all five leaf traits had similar model performance compared to the laboratory spectral models with R^2 of 0.50–0.89 and RMSEP of 5.7–18.3% (Fig. 6). The highest performing general model was the water content prediction model utilizing HyspIRI (R^2 = 0.89 and RMSEP = 5.7%), which is consistent with the Full spectrum having the highest model performance with the laboratory spectra. The cellulose general model followed with R^2 = 0.70 and

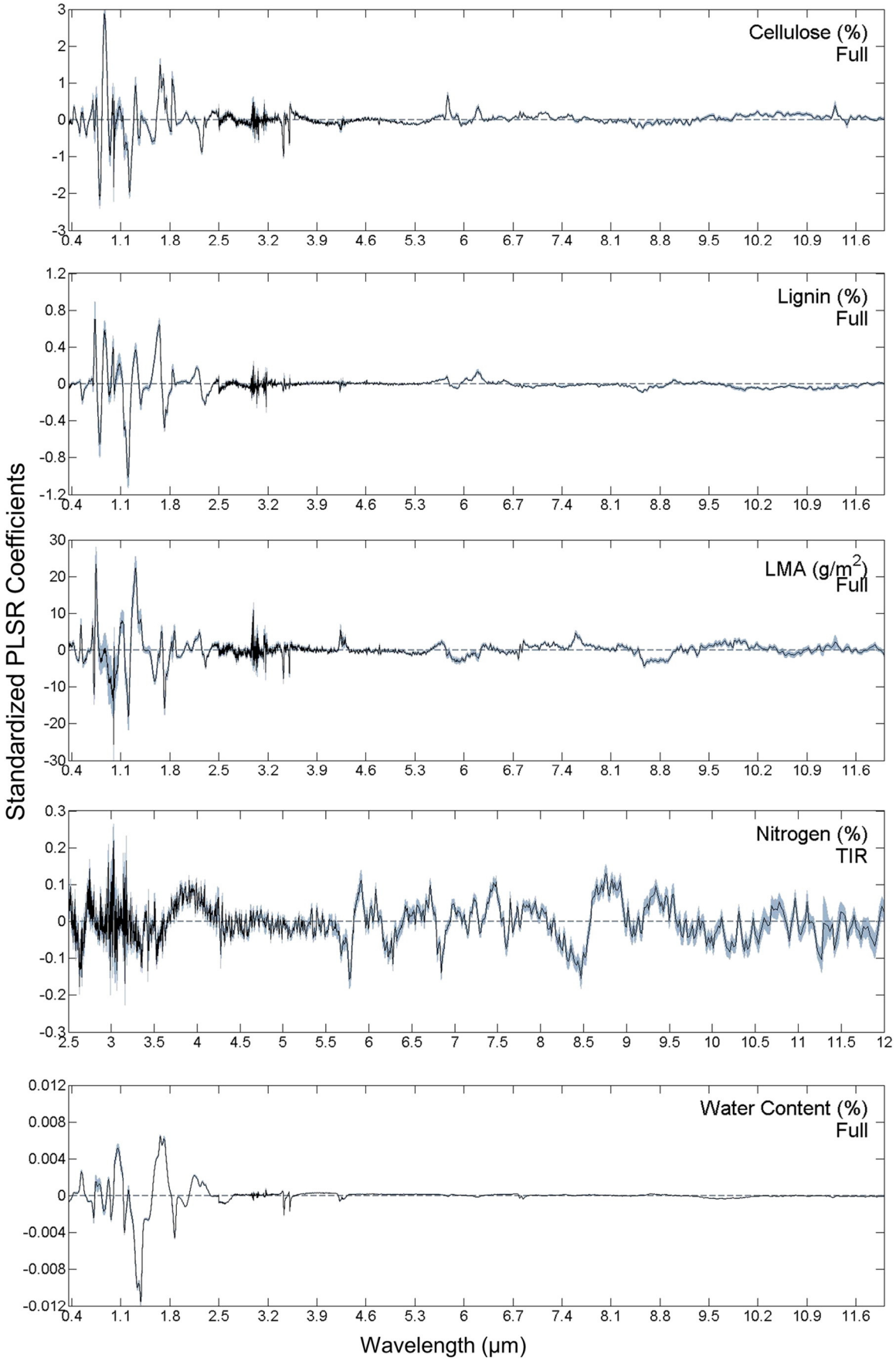

Fig. 5. Standardized PLSR coefficients from best performing laboratory general models indicating the magnitude and direction of influence of each wavelength; gray shading denotes one standard deviation.

Table 4
The ten wavelengths with the largest magnitude PLSR coefficients for laboratory general models ordered from largest to smallest magnitude. Wavelength units are in micrometers.

Cellulose	Lignin	LMA	Nitrogen	Water content
0.865	0.729	0.742	3.031	1.665
0.870	1.650	1.313	3.017	1.717
0.876	0.866	1.310	2.504	1.053
0.857	0.870	2.992	3.177	1.060
0.895	0.863	1.383	12.996	1.058
1.662	0.875	1.116	2.965	1.009
1.707	0.991	1.118	2.748	0.537
1.832	1.313	1.122	8.759	2.155
1.841	0.985	1.126	3.141	0.924
1.311	0.982	1.358	3.034	0.918

RMSEP = 13.1%. The lignin, LMA, and nitrogen general models had similar model performance with R^2 = 0.50, 0.56, 0.56 and RMSEP = 17.7, 18.3, 18.1% respectively. In general sensor-simulated spectra models lost model performance (~2.5% RMSEP) compared to the laboratory spectra models.

For sensor-simulated models, we again used the standardized PLSR coefficients to identify the regions of the spectrum that were important to the general model calibrations (Table 6; Fig. 7). For all leaf traits, the coefficients with the largest magnitude lie in the 0.7–1.3 μm spectral range. The eight TIR bands of HyspIRI used to predict cellulose, LMA, nitrogen, and water content had generally low magnitude coefficients with the band at 3.98 μm consistently having the largest magnitude coefficient. Model coefficients differed between seasonal (Fig. A6) and leaf-form models (Fig. A7) and resulted in different sets of largest magnitude PLSR coefficients. Scaling from laboratory spectra to sensor simulated spectra changed the PLSR coefficients so the wavelengths that are most influential for prediction differ between finer and coarser spectral resolution (Fig. 8).

4. Discussion

Our results for sixteen common California plant species demonstrate the ability of VSWIR and TIR spectra to characterize a wide range of foliar traits between leaf forms and across seasons. We show that the ability to predict foliar traits using laboratory spectra can be extended to the reduced spectral resolution of current and proposed sensors. Before a generalizable model can be implemented, an understanding of the variability that might be present in the dataset is required. We developed seasonal and leaf form specific models to explore if a generalizable model is able to predict leaf traits accurately across this variability. We demonstrate for plant species ranging from trees to chaparral shrubs that seasonal and leaf form models vary in trait prediction capabilities. A general model capturing seasonal and leaf form variation was possible for all traits, but only cellulose and water content had model performance of $R^2 > 0.70$ and RMSEP < 15%. Each leaf trait PLSR prediction model performed differently across seasons and between leaf forms.

Cellulose forms one third to one half of the dry weight in most plants, which is mirrored in our dataset, making it the most abundant organic compound in terrestrial ecosystems (Elvidge, 1988). In spectroscopy, this translates into a larger spectral signal that should allow for higher prediction capabilities. For example in our analysis, cellulose predictions had the second highest performance of the five traits. Cellulose is one of the few leaf traits being analyzed in other studies using the TIR spectrum because of strong absorption features in this region (Ribeiro da Luz, 2006; Ribeiro da Luz and Crowley, 2007). This supports our model results in which the Full and HyspIRI spectra were used frequently. Five of the eight TIR bands in HyspIRI are associated with cellulose absorption features supporting the use of the HyspIRI spectrum in best performing models (Elvidge, 1988). However, large magnitude PLSR coefficients in the VSWIR suggest that this spectral range is more influential in cellulose predictions, which is a possible

Table 5
Best performing models using sensor-simulated spectra for each leaf trait and model category. Performance was determined using external independent validation results. N is total number of samples, N_{val} is the number of samples set aside to calculate validation statistics, and *h* is the number of factors used to build PLSR models.

	Model					Internal validation		External validation	
	Category	Spectrum	N	N_{val}	*h*	R^2 (S.D.)	RMSEP (S.D.)	R^2	RMSEP
Cellulose	General	HyspIRI	284	57	13	0.53 (0.08)	15.38 (2.48)	0.70	13.06
	Broadleaf	AVIRIS	194	37	12	0.46 (0.11)	18.12 (3.25)	0.60	17.01
	Needleleaf	AVIRIS	90	17	12	0.53 (0.16)	20.60 (4.48)	0.69	17.24
	Spring	HyspIRI	96	19	12	0.56 (0.10)	19.87 (4.71)	0.91	10.25
	Summer	HyspIRI	95	18	10	0.56 (0.12)	17.50 (3.50)	0.52	21.45
	Fall	HyspIRI	93	18	13	0.57 (0.10)	18.69 (3.86)	0.72	16.56
Lignin	General	AVIRIS	284	56	14	0.37 (0.08)	17.39 (2.42)	0.50	17.65
	Broadleaf	HyspIRI	194	39	15	0.45 (0.10)	20.25 (3.61)	0.42	19.38
	Needleleaf	HyspIRI	90	18	14	0.29 (0.14)	23.69 (5.58)	0.57	17.90
	Spring	HyspIRI	96	20	14	0.60 (0.11)	16.71 (2.75)	0.67	14.65
	Summer	HyTES	95	18	13	0.48 (0.12)	20.00 (3.46)	0.56	17.09
	Fall	AVIRIS	93	18	10	0.27 (0.13)	28.83 (7.30)	0.46	23.18
LMA	General	HyspIRI	265	53	11	0.57 (0.07)	14.49 (2.01)	0.56	18.31
	Broadleaf	HyspIRI	195	39	12	0.51 (0.09)	18.01 (2.97)	0.69	14.70
	Needleleaf	HyTES	70	14	11	0.14 (0.10)	29.14 (10.63)	0.37	26.39
	Spring	AVIRIS	90	17	10	0.50 (0.11)	19.25 (3.58)	0.80	16.99
	Summer	HyTES	90	16	12	0.35 (0.12)	27.59 (4.54)	0.82	15.15
	Fall	HyspIRI	85	17	11	0.58 (0.13)	19.78 (4.60)	0.53	24.20
Nitrogen	General	HyspIRI	284	56	11	0.45 (0.10)	20.24 (3.07)	0.56	18.13
	Broadleaf	AVIRIS	195	36	12	0.46 (0.10)	14.75 (2.89)	0.55	19.32
	Needleleaf	HyTES	89	17	10	0.13 (0.11)	21.02 (7.06)	0.26	24.33
	Spring	AVIRIS	96	18	12	0.72 (0.13)	17.29 (4.62)	0.82	17.39
	Summer	HyTES	96	18	11	0.16 (0.12)	45.77 (9.10)	0.22	26.97
	Fall	AVIRIS	92	18	11	0.35 (0.15)	30.69 (7.80)	0.33	30.42
Water content	General	HyspIRI	284	53	10	0.60 (0.12)	11.75 (1.99)	0.89	5.75
	Broadleaf	AVIRIS	194	37	8	0.63 (0.11)	13.06 (2.59)	0.78	8.59
	Needleleaf	AVIRIS	90	18	7	0.67 (0.08)	11.72 (2.16)	0.86	9.03
	Spring	HyspIRI	96	18	11	0.67 (0.11)	16.50 (3.42)	0.71	16.78
	Summer	AVIRIS	95	16	10	0.38 (0.19)	19.81 (5.82)	0.75	10.66
	Fall	AVIRIS	93	18	9	0.67 (0.17)	14.14 (3.90)	0.80	12.59

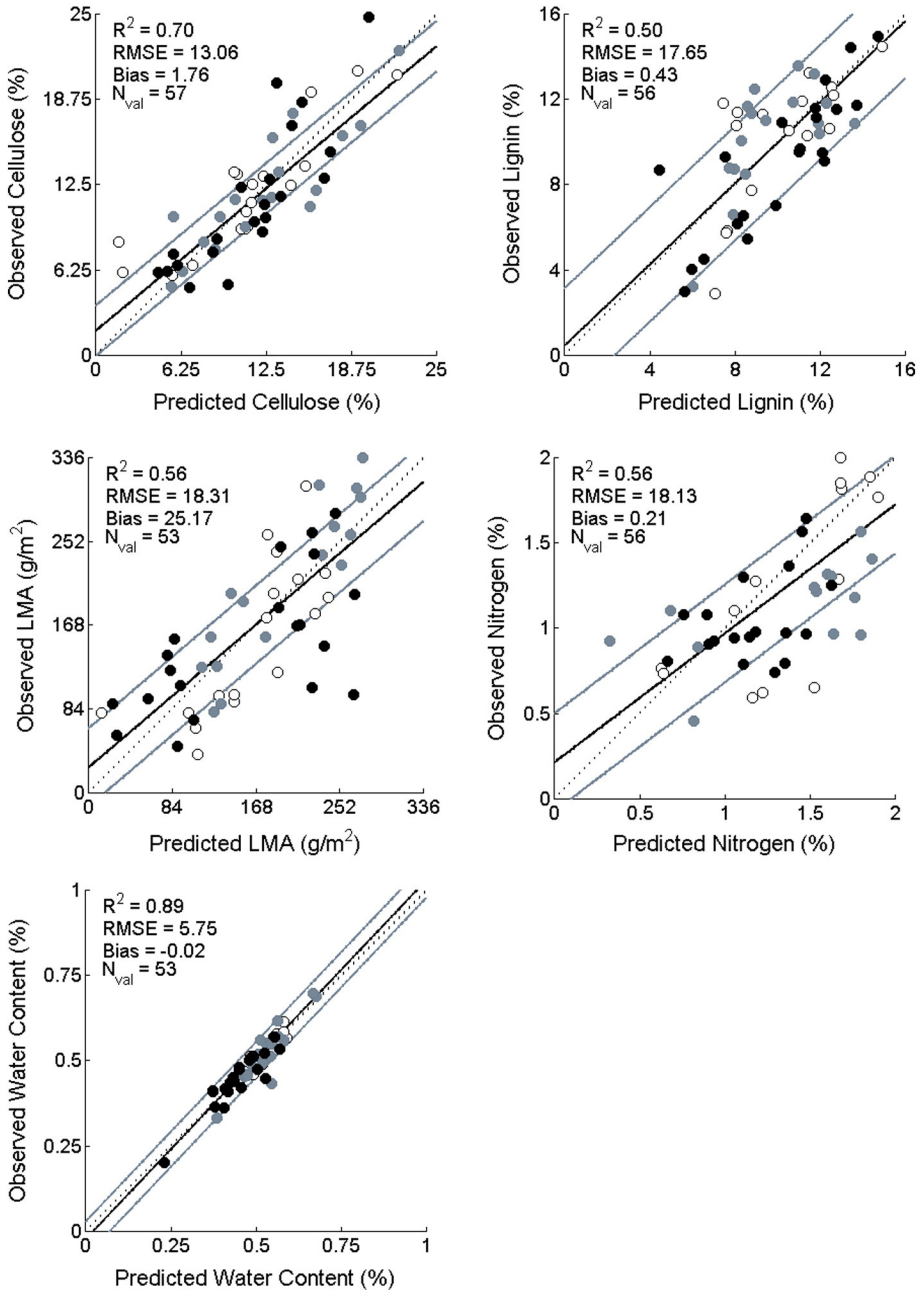

Fig. 6. Independent validation results for the best performing sensor-simulated general PLSR models. Dark line denotes regression line, light gray lines show the 95% confidence intervals of the models, and dashed line shows the 1:1 line. Black symbols denote spring season samples, gray symbols denote summer, and white symbols denote fall.

Table 6
The ten wavelengths with the largest magnitude PLSR coefficients for sensor-simulated general models ordered from largest to smallest magnitude. Wavelength units in micrometers.

Cellulose	Lignin	LMA	Nitrogen	Water content
0.860	1.158	1.262	1.205	1.033
1.661	0.985	1.148	0.801	1.062
0.753	0.733	0.743	1.014	1.721
1.711	1.632	1.791	1.592	0.733
1.158	0.879	1.691	1.043	0.927
1.139	1.005	2.227	1.721	1.661
0.985	1.651	0.850	0.927	1.592
1.751	0.860	0.956	0.995	0.811
1.262	1.110	0.694	1.062	0.792
1.801	1.602	2.187	0.550	1.215

explanation for the lack of best models using HyTES despite the fact that there are strong cellulose absorption features in the TIR. While there were significant differences between leaf form and seasons in the analytically measured dataset, the cellulose general model was able to capture this variability with high performance ($R^2 = 0.70$ and RMSEP = 13.1%. In comparison with studies from other ecosystems using AVIRIS, Asner et al. (2011) reported an $R^2 = 0.77$ and RMSE = 6.4%, Bolster et al. (1996) reported an $R^2 = 0.89$, and Singh et al. (2015) reported an $R^2 = 0.49$ and RMSE = 1.8%.

On the other hand, lignin had some of the poorest model performance compared to the other leaf traits in this study (General AVIRIS model $R^2 = 0.50$ and RMSEP = 17.65%). Additionally, these results were lower than reported in the literature. For example, Asner et al. (2011) using VSWIR data reported an $R^2 = 0.62$ and RMSEP = 10.0%, Martin and Aber (1997) developed models with $R^2 = 0.77$, and Singh et al. (2015) reported models with $R^2 = 0.74$ and RMSEP = 2.3%. In

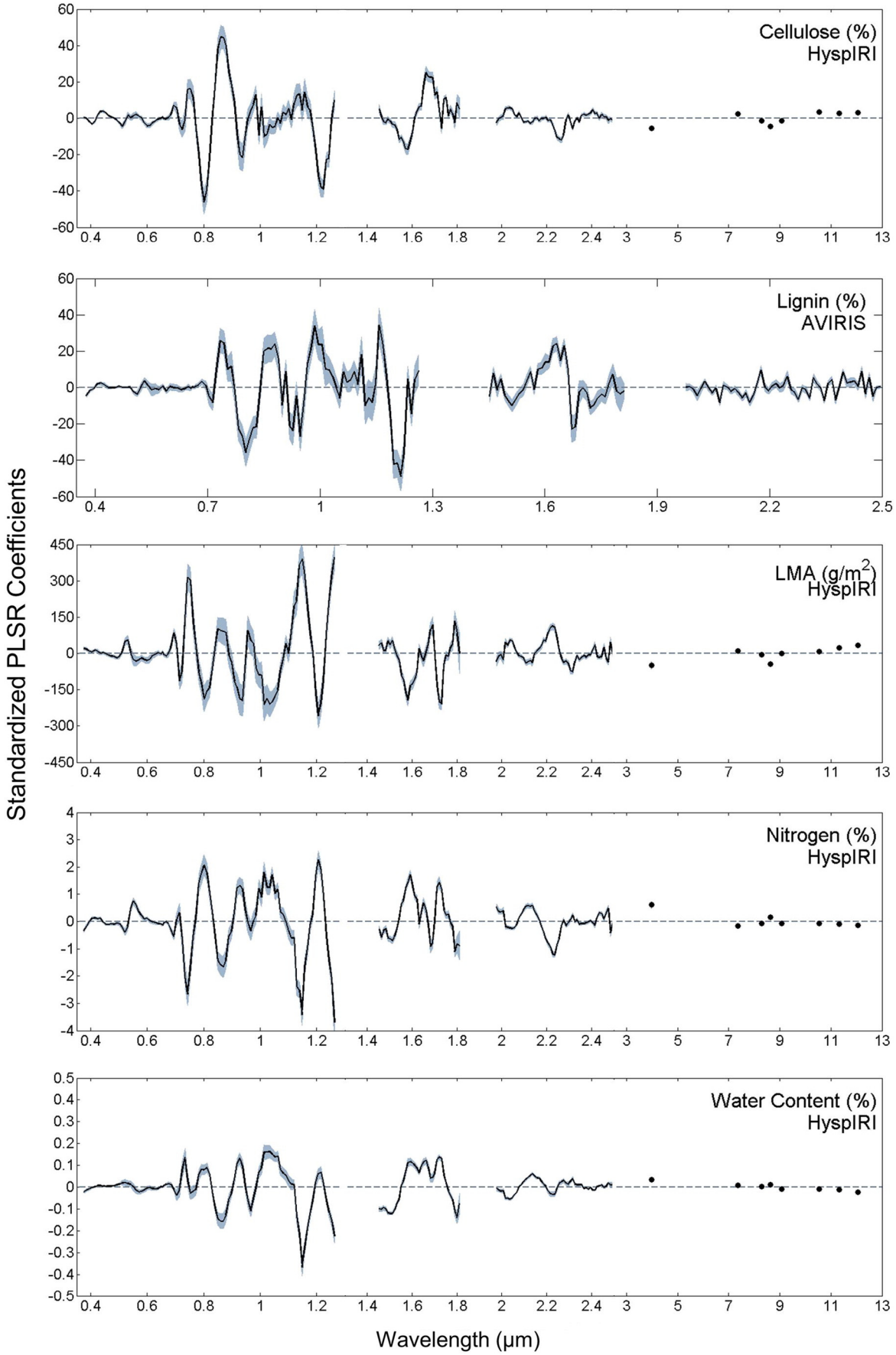

Fig. 7. Standardized PLSR coefficients from best performing sensor-simulated general models indicating the magnitude and direction of influence of each wavelength; gray shading denotes one standard deviation.

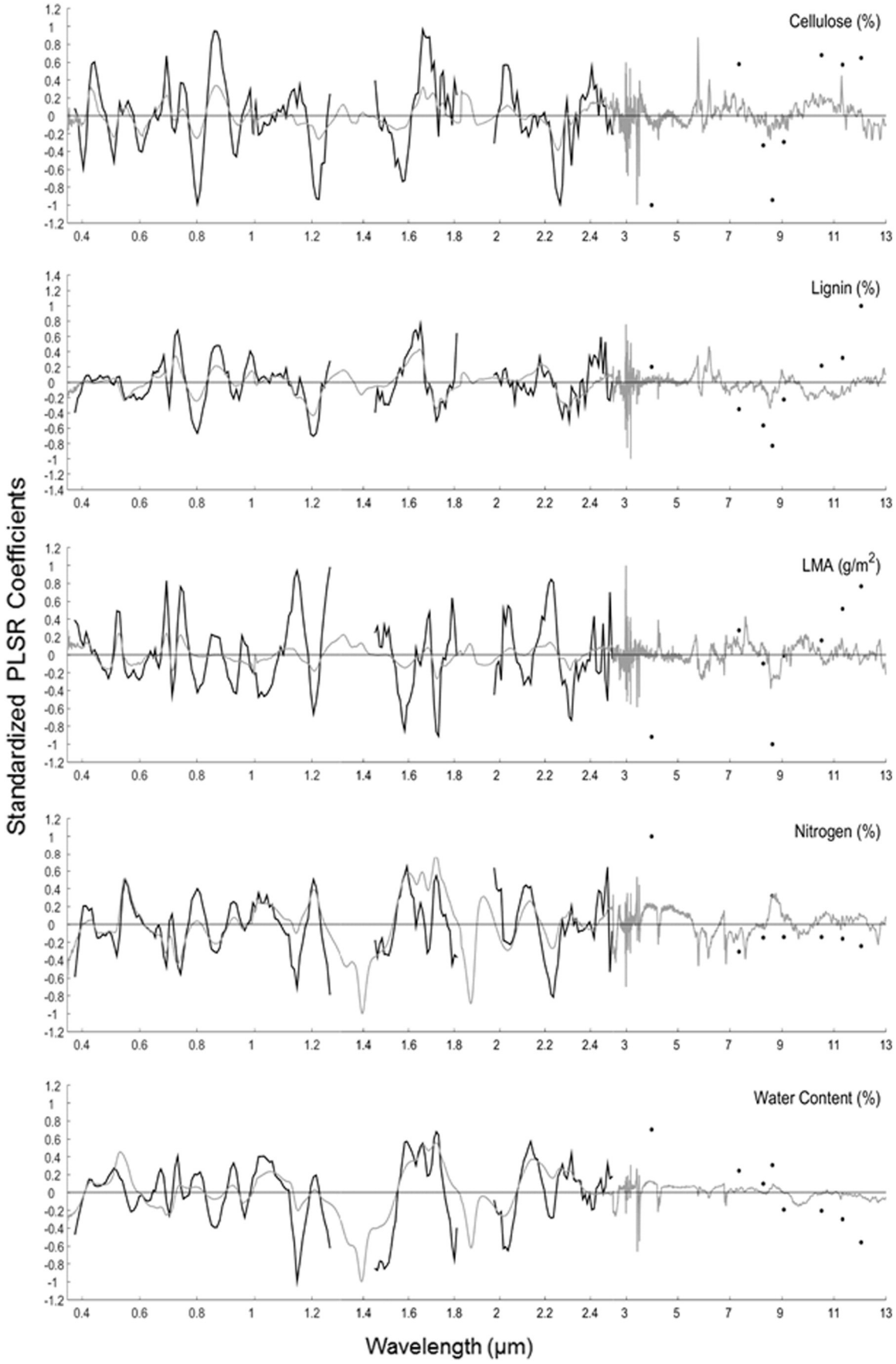

Fig. 8. Standardized PLSR coefficients from Full spectrum (gray line) and HyspIRI sensor-simulated (black line) general models indicating the magnitude and direction of influence of each wavelength.

our study, lignin samples were statistically different between leaf forms and among seasons, and the PLSR models performed worse when there was high variability within a model category. As a result, the lignin general model had lower model performance compared to spring and summer seasons. While other studies have developed a generalized model for lignin prediction, our results demonstrate that a generalized model is not able to capture the seasonal variation in lignin for the California trees and shrubs studied here. The majority of lignin prediction models used the Full and HyspIRI spectra with large magnitude PLSR coefficients in the TIR lying in close proximity to known absorption features of lignin residing in wavelengths 2.5–13 μm with the strongest and largest absorptions in the mid infrared (MIR) range of 2.5 and 6 μm (Elvidge, 1988). Lignin and cellulose, despite not being correlated in this dataset, share many of the same absorption wavelengths in the literature, which is reflected in the wavelengths with the largest PLSR coefficients (Curran, 1989; Elvidge, 1988).

LMA is a key trait for plant growth and can be used as an indicator of plant strategies of resource acquisition and competition (Lambers and Poorter, 2004; Westoby, 1998). However, as also seen in our dataset, plant species exhibit a wide variation in LMA between leaf forms and with seasonal growth (Poorter et al., 2009). This variability translated into a wide amount of variation in model performance between seasonal and leaf form models ($R^2 = 0.37–0.82$ and RMSEP = 14.7–26.4%). We see this reflected in the literature with other studies encompassing similar ranges in R^2 values from 0.79 to 0.93 using the VSWIR (Asner et al., 2009; Asner et al., 2011; Asner and Martin, 2008; Doughty et al., 2011). For the sixteen plant species studied here, a generalized model did not sufficiently capture the variability, resulting in lower model performance compared to models specifically developed for seasons and leaf forms. LMA was unique among the leaf traits analyzed in this study because its best models used HyspIRI or HyTES the majority of the time. The largest magnitude PLSR coefficients matched known absorption features of starches, lignin, and cellulose (Curran, 1989; Elvidge, 1988). The TIR spectrum is also characterized by cutin, waxes, silica, and other leaf structural component absorption features (Ribeiro da Luz and Crowley, 2007). PLSR coefficients from HyTES models exhibit some of these absorption features, suggesting that when predicting LMA, absorption features of structural components of leaves assist prediction.

Nitrogen is the key substance that limits where and how well plants grow because it is necessary for the development of proteins (King, 2011). Due to nitrogen's essential nature, it has been one of the most widely predicted leaf traits throughout the world (Asner et al., 2011; Bolster et al., 1996; Dury and Turner, 2001). Our models had lower performance compared to many in the literature, which might be due to the type of plant species analyzed or the smaller range of nitrogen content present in the dataset. Most known major absorption features of nitrogen are located in the VSWIR (Curran, 1989). This is consistent with our model results which predominantly used the VSWIR or AVIRIS spectrum, and the largest PLSR coefficients are present in the VSWIR spectrum. However, the Full, TIR, HyspIRI, and HyTES spectral ranges also yielded best models showing that the TIR spectrum contains spectral information that improved prediction of nitrogen. While nitrogen does not have known absorption features in the TIR, the proteins comprised of nitrogen do have absorption features in this spectral range. For example, the protein ribulose 1-5-biphosphate carboxylase (RuBisCo) accounts for 30–50% of the nitrogen in fresh leaves and has absorption features present at wavelengths 7.5–13 μm (Elvidge, 1988).

In fresh green leaves, water is a major constituent and can account for 40–80% of weight (Elvidge, 1988). This contributed to a strong spectral signal of water content in our study that resulted in the highest prediction results with R^2 value >0.71 and RMSEP < 16.8%. The HyspIRI spectrum yielded the highest general model performance, demonstrating the importance of the TIR spectrum for predicting water content when there is a wide range of variability present in the dataset. Water content is one of the few leaf traits being actively studied in the TIR spectrum. Ullah et al. (2014) analyzed leaf water content in different portions of the Full spectrum (0.39–14.0 μm) by running PLSR models and found that the MIR (2.5–6 μm) spectral region resulted in the highest agreement. Our PLSR coefficients have the largest magnitudes in VSWIR with some absorption features in the MIR for the Full spectrum and 3.98 μm for HyspIRI. However, the HyTES spectral range (7.5–12 μm) did not result in high model performance because it does not contain the MIR. While there were significant differences between seasonal leaf water content in our analytically measured dataset, the general model was able to capture the variability with high performance ($R^2 = 0.89$ and RMSEP = 5.75%). Our model results reflect similar studies in the literature. Asner et al. (2011) reports $R^2 = 0.88$ and RMSEP = 5.3%, and Ullah et al. (2014) reports $R^2 = 0.96$ and RMSEP = 4.7%.

Model comparisons were conducted using external validation results that were calculated using a randomly selected 20% of the dataset. In an unusual circumstance, internal validation R^2 model results were consistently lower than external validation R^2 model results. RMSEP is a better estimate of model performance and allows for comparison between models because it is normalized by the percentage of the response data range. The RMSEP results for external and internal validation do not show the same pattern as R^2 results. The consistently higher external validation results for R^2 are probably due to random subsampling.

While sensor-simulated models assess how well reduced spectral resolution can discriminate leaf traits, there are other factors to consider when up-scaling from laboratory spectra to the imagery that would be available using HyspIRI. Using Full spectrum spectroscopy on a global scale poses several challenges caused by the atmosphere, lighting geometry, temperature-emissivity separability, canopy structure, and variability of vegetation characteristics. While we attempted to correct for the atmosphere's effect by removing water vapor regions of the spectrum, ultimately there is still enough interference from the atmospheric attenuation and emission to obscure surface spectra (Young et al., 2002). Emissivity retrievals are complicated by temperature variations, leaf angle, and shading inside a canopy, which need to be retrieved using atmospheric compensation and temperature-emissivity separation methods (Ribeiro da Luz and Crowley, 2010). Our study attempted to capture a wide range of leaf variations by sampling current and last year's growth, replicates of species, and seasons. However, this study was focused on only three sites in California and is not representative of the total variation that would be captured by a global mission. While there are challenges to overcome before using Full spectrum spectroscopy on a global scale, this study does present a foundation for understanding how the Full spectrum can improve prediction of vegetation properties using airborne and satellite sensors.

This study presents opportunities not only for the proposed satellite HyspIRI, but also for airborne and satellite sensors currently deployed. At the airborne level, the NASA HyspIRI Airborne Preparatory campaign, using the AVIRIS and MODIS/ASTER (MASTER) sensors, will have collected imagery for 2013–2015 over California, providing Full spectrum imagery that could be used to predict California's diverse natural vegetation traits (Green et al., 2013). At the satellite level, Full spectrum imagery would also be possible using two sensors that are set to launch in the near future. The Environmental Mapping and Analysis Program (EnMAP) is a German imaging spectrometer that will measure 420 to 1000 nm and 900 to 2450 nm (VSWIR) and is scheduled to be launched in 2018 (Stuffler et al., 2007). For the TIR spectral range, the ECOsystem Spaceborne Thermal Radiometer Experiment on Space Station (ECOSTRESS) sensor will be launched between 2017 and 2019 on the International Space Station (ISS) (Hook, 2014). This sensor would capture imagery with five bands in the Thermal Infrared window (8–12.5 μm). The imagery available from these two sensors would allow for Full spectrum vegetation trait prediction with global coverage. While the HyspIRI sensor would provide simultaneously collected VSWIR-TIR data, the launch date for this project is not set. The sensors

mentioned on the airborne and satellite platforms provide more present opportunities to use the Full spectrum to enhance vegetation trait predictions.

5. Conclusions

The combination of VSWIR and TIR used to predict leaf traits increased the prediction capabilities of PLSR models compared to using VSWIR alone, signifying that the inclusion of TIR data would improve predictions of foliar traits, which varied widely among the sixteen plant species studied. When using sensor-simulated spectra to predict leaf traits, simulated HyspIRI spectra produced the majority of the best performing models. While there are only eight additional bands in the TIR for the HyspIRI spectrum, these provided spectral signatures that ultimately resulted in improved model performance over AVIRIS alone. This is a key finding, in as almost all previous studies have used VSWIR or TIR but not both.

To harness the temporal and spatial scales available using aerial and space-borne sensors, generalized and transportable models must be developed to accurately map canopy biochemical and biophysical properties. We found that model precision varied by season as well as across leaf forms which ultimately can inform researchers about potential sources of error when developing generalizable models. For the prediction of lignin and LMA, the variability among seasons and between leaf forms results in a low performing general model. However, it was possible to develop a general model that captured seasonal variation for cellulose, nitrogen, and water content.

In summary these results indicate that the TIR spectrum could augment the VSWIR in advancing identification of leaf biochemical and physical properties on large spatial and temporal scales. This research highlights the benefits of the proposed HyspIRI satellite with a VSWIR imaging spectrometer and a TIR multi-spectral imager for estimation of vegetation traits and represents an important step in evaluating the full potential of the HyspIRI satellite. Advancing this research beyond the leaf level will further determine the potential use of the Full spectrum for predicting canopy traits across the globe.

Acknowledgements

We wish to thank Dr. Carla D'Antonio for the use of her laboratory and equipment. This research was supported by NASA grant NNX12AP08G, *HyspIRI discrimination of plant species and functional types along a strong environmental-temperature gradient*. A portion of this work was carried out at the Jet Propulsion Laboratory/California Institute of Technology, Pasadena, California, under contract with the National Aeronautics and Space Administration. Dr. Cibele Hummel do Amaral thanks the São Paulo Research Foundation (# 10/51718-0) for supporting her stay in the United States.

Appendix A. Supplementary data

Supplementary data associated with this article can be found in the online version at doi:http://doi.dx.org/10.1016/j.rse.2016.08.003.

References

Abrams, M.J., Hook, S.J., 2013. NASA's Hyperspectral Infrared Imager (HyspIRI). Thermal Infrared Remote Sensing Edited by C. Kuenza and S, Dech, Springer (527 p).
Arnold, S.L., Schepers, J.S., 2004. A simple roller-mill grinding procedure for plant and soil samples. Commun. Soil Sci. Plant Anal. 35 (3–4), 537–545.
Asner, G.P., Martin, R.E., 2008. Spectral and chemical analysis of tropical forests: scaling from leaf to canopy levels. Remote Sens. Environ. 112 (10), 3958–3970 http://doi.org/10.1016/j.rse.2008.07.003.
Asner, G.P., Martin, R.E., Ford, A.J., Metcalfe, D.J., Liddell, M.J., 2009. Leaf chemical and spectral diversity in Australian tropical forests. Ecol. Appl. 19 (1), 236–253.
Asner, G.P., Martin, R.E., Knapp, D.E., Tupayachi, R., Anderson, C., Carranza, L., Martinez, P., Houcheime, M., Sinca, F., Weiss, P., 2011. Spectroscopy of canopy chemicals in humid tropical forests. Remote Sens. Environ. 115 (12), 3587–3598.
Asner, G.P., Martin, R.E., Anderson, C.B., Knapp, D.E., 2015. Quantifying forest canopy traits: imaging spectroscopy versus field survey. Remote Sens. Environ. 158, 15–27. http://dx.doi.org/10.1016/j.rse.2014.11.011.
Atkin, O.K., Bloomfield, K.J., Reich, P.B., Tjoelker, M.G., Asner, G.P., Bonal, D., ... Rowland, L.M., 2015. Global variability in leaf respiration in relation to climate, plant functional types and leaf traits. New Phytol. 206, 614–636.
Baldridge, A.M., Hook, S.J., Grove, C.I., Rivera, G., 2009. The ASTER spectral library version 2.0. Remote Sens. Environ. 113, 711–715.
Berk, A., Anderson, G.P., Acharya, P.K., Bernstein, L.S., Muratov, L., Lee, J., Fox, M., Adler-Golden, S.M., Chetwynd, J.H., Hoke, M.L., Lockwood, R.B., Gardner, J.A., Cooley, T.W., Borel, C.C., Lewis, P.E., 2005. MODTRAN™ 5, a reformulated atmospheric band model with auxiliary species and practical multiple scattering options: update. In: Sylvia, S.S., Lewis, P.E. (Eds.), Algorithms and Technologies for Multispectral, Hyperspectral, and Ultraspectral Imagery XI. Bellingham, WA, Proceedings of SPIE.
Bolster, K.L., Martin, M.E., Aber, J.D., 1996. Determination of carbon fraction and nitrogen concentration in tree foliage by near infrared reflectance: a comparison of statistical methods. Can. J. For. Res. 26, 590–600.
Countryman, C.M., Dean, W.H., 1979. Measuring moisture content in living chaparral: a field user's manual. General Technical Report PSW-36. (27 pp.). USDA, Forest Service Pacific Southwest Forest and Range Experiment Station, Berkeley, CA.
Curran, P.J., 1989. Remote sensing of foliar chemistry. Remote Sens. Environ. 30 (3), 271–278.
Dahlgren, R.A., Boettinger, J.L., Huntington, G.L., Amundson, R.G., 1997. Soil development along an elevational transect in the western Sierra Nevada, California. Geoderma 78, 207–236.
Dennison, P.E., Thorpe, A.K., Pardyjak, E.R., Roberts, D.A., Qi, Y., Green, R.O., Bradley, E.S., Funk, C.C., 2013. High spatial resolution mapping of elevated atmospheric carbon dioxide using airborne imaging spectroscopy: radiative transfer modeling and power plant plume detection. Remote Sens. Environ. 139, 116–129.
Doughty, C.E., Asner, G.P., Martin, R.E., 2011. Predicting tropical plant physiology from leaf and canopy spectroscopy. Oecologia 165 (2), 289–299.
Dury, S.J., Turner, B.J., 2001. Nutrient estimation of eucalypt foliage derived from hyperspectral data. IEEE Int. Geosci. Remote Sens. Symp. 2, 774–776.
Elvidge, C.D., 1988. Thermal infrared reflectance of dry plant materials: 2.5–20.0 μm. Remote Sens. Environ. 26, 265–285.
Fabre, S., Lesaignoux, A., Olioso, A., Briottet, X., 2011. Influence of water content on spectral reflectance of leaves in the 3–15 μm domain. IEEE Geosci. Remote Sens. Lett. 8 (1), 143–147.
Feilhauer, H., Asner, G.P., Martin, R.E., Schmidtlein, S., 2010. Brightness-normalized partial least squares regression for hyperspectral data. J. Quant. Spectrosc. Radiat. Transf. 111, 1947–1957.
Ferwerda, J.G., Skidmore, A.K., Mutanga, O., 2005. Nitrogen detection with hyperspectral normalized ratio indices across multiple plant species. Int. J. Remote Sens. 26 (18), 4083–4095.
Gao, B.C., Goetz, A.F.H., 1995. Retrieval of equivalent water thickness and information related to biochemical components of vegetation canopies from AVIRIS data. Remote Sens. Environ. 52, 155–162.
Green, R.O., Eastwood, M.L., Sarture, C.M., Chrien, T.G., Aronsson, M., Chippendale, B.J., Faust, J.A., Pavri, B.E., Chovit, C.J., Solis, M., Olah, M.R., Williams, O., 1998. Imaging spectroscopy and the Airborne Visible/Infrared Imaging Spectrometer (AVIRIS). Remote Sens. Environ. 65, 227–248.
Green, R.O., McCubbin, I., Hook, S.J., 2013. HyspIRI preparatory airborne campaign. Proceedings of HyspIRI Workshop 2013 (Pasadena, California, 16 October).
Haaland, D.M., Thomas, E.V., 1988. Partial least-squares methods for spectral analyses. 1. Relation to other quantitative calibration methods and the extraction of qualitative information. Anal. Chem. 60 (11), 1193–1202.
Hatfield, R., Fukushima, R.S., 2005. Can lignin be accurately measured? Crop Sci. 45 (3), 832–839.
Hook, S.J., 2014. ECOsystem spaceborne thermal radiometer experiment on space station. Proceedings of HyspIRI Workshop 2014 (Pasadena, California, 15 October).
Hook, S.J., Johnson, W.R., Abrams, M.J., 2013. NASA's hyperspectral thermal emission spectrometer. In: Kuenzer, C., Dech, S. (Eds.), Thermal Infrared Remote Sensing: Sensors, Methods, Applications Vol. 17. Springer, Dordrecht, pp. 93–115.
Johnson, W., 2015. Personal Correspondence. NASA Jet Propulsion Laboratory, Pasadena, CA.
Jurik, T.W., 1986. Temporal and spatial patterns of specific leaf weight in successional northern hardwood tree species. American Journal of Botany]–>Am. J. Bot. 73 (8), 1083–1092.
King, J., 2011. Reaching for the Sun: How Plants Work. NY. Cambridge University Press, New York.
Lambers, H., Poorter, H., 2004. Inherent variation in growth rate between higher plants: a search for physiological causes and ecological consequences. Adv. Ecol. Res. 34, 283–362 http://doi.org/10.1016/S0065-2504(03)34004-8.
Lawler, I.R., Aragones, L., Berding, N., Marsh, H., Foley, W., 2006. Near-infrared reflectance spectroscopy is a rapid, cost-effective predictor of seagrass nutrients. J. Chem. Ecol. 32 (6), 1353–1365.
Lee, C.M., Cable, M.L., Hook, S.J., Green, R.O., Ustin, S.L., Mandl, D.J., Middleton, E.M., 2015. An introduction to the NASA Hyperspectral InfraRed Imager (HyspIRI) mission and preparatory activities. Remote Sens. Environ. 167, 6–19. http://dx.doi.org/10.1016/j.rse.2015.06.012.
Mahall, B.E., Davis, F.W., Tyler, C.M., 2005. Final Report of the Santa Barbara County Oak Restoration Program: August 1994–August 2005. County of Santa Barbara Department of Planning and Development. Energy Division, University of California Santa Barbara.
Martens, H., Karstang, T., Naes, T., 1987. Improved selectivity in spectroscopy by multivariate calibration. J. Chemom. 1, 201–219.
Martin, M.E., Aber, J.D., 1997. High spectral resolution remote sensing of forest canopy lignin, nitrogen, and ecosystem processes. Ecol. Appl. 7 (2), 431–443.
Mauffette, Y., Oechel, W.C., 1989. Seasonal variation in leaf chemistry of the coast live oak *Quercus agrifolia* & and implications for the California oak moth *Phryganidia californica*. Oecologia 79, 439–445.

Ollinger, S.V., Smith, M.L., Martin, M.E., Hallett, R.a., Goodale, C.L., Aber, J.D., 2002. Regional variation in foliar chemistry and N cycling among forests of diverse history and composition. Ecology 83 (2), 339–355.
Poorter, H., Niinemets, U., Poorter, L., Wright, I.J., Villar, R., 2009. Causes and consequences of variation in leaf mass per area (LMA): a meta-analysis. New Phytologist 182 (3), 565–588.
Quinn, R.D., Keeley, S.C., 2006. Introduction to California Chaparral. University of California Press, Los Angeles, California.
Ribeiro da Luz, B., 2006. Attenuated total reflectance spectroscopy of plant leaves: a tool for ecological and botanical studies. New Phytologist 172 (2), 305–318.
Ribeiro da Luz, B., Crowley, J.K., 2007. Spectral reflectance and emissivity features of broad leaf plants: prospects for remote sensing in the thermal infrared (8.0–14.0 μm). Remote Sens. Environ. 109 (4), 393–405.
Ribeiro da Luz, B., Crowley, J.K., 2010. Identification of plant species by using high spatial and spectral resolution thermal infrared (8.0–13.5 μm) imagery. Remote Sens. Environ. 114 (2), 404–413.
Richardson, A.D., Berlyn, G.P., Gregoire, T.G., 2001. Spectral reflectance of *Picea rubens* (Pinaceae) and *Abies balsamea* (Pinaceae) needles along an elevation gradient, Mt. Moosilauke, New Hampshire, USA. Am. J. Bot. 88 (4), 667–676.
Salisbury, J.W., 1986. Preliminary measurements of leaf spectral reflectance in the 8.0–14.0 μm region. Int. J. Remote Sens. 7 (12), 1879–1886.
Schneider, C.A., Rasband, W.S., Eliceiri, K.W., 2012. NIH image to ImageJ: 25 years of image analysis. Nat. Methods 9 (7), 671–675.
Serbin, S.P., Dillaway, D.N., Kruger, E.L., Townsend, P.A., 2012. Leaf optical properties reflect variation in photosynthetic metabolism and its sensitivity to temperature. J. Exp. Bot. 63 (1), 489–502 http://doi.org/10.1093/jxb/err294.
Serbin, S.P., Singh, A., McNeil, B.E., Kingdon, C.C., Townsend, P.A., 2014. Spectroscopic determination of leaf morphological and biochemical traits for northern temperate and boreal tree species. Ecol. Appl. 24 (7), 1651–1669 http://doi.org/10.1890/13-2110.1.
Shenk, J.S., Westerhaus, M.O., Hoover, M.R., 1979. Analysis of forages by infrared reflectance. J. Dairy Sci. 62 (5), 807–812.
Singh, A., Serbin, S.P., McNeil, B.E., Kingdon, C.C., Townsend, P.A., 2015. Imaging spectroscopy algorithms for mapping canopy foliar chemical and morphological traits and their uncertainties. Ecol. Appl. 25 (8), 2180–2197 http://doi.org/10.1890/14-2098.1.
Smith, M.L., Martin, M.E., Plourde, L., Ollinger, S.V., 2003. Analysis of hyperspectral data for estimation of temperature forest canopy nitrogen concentration: comparison between an airborne (AVIRIS) and a spaceborne (Hyperion) sensor. IEEE Trans. Geosci. Remote Sens. 41 (6), 1332–1337.
Stuffler, T., Kaufmann, C., Hofer, S., Förster, K.P., Schreier, G., Mueller, A., Eckardt, A., Bach, H., Penné, B., Benz, U., Haydn, R., 2007. The EnMAP hyperspectral imager—an advanced optical payload for future applications in Earth observation programmes. Acta. Astronautica 61 (1–6), 115–120. http://dx.doi.org/10.1016/j.actaastro.2007.01.033.
Ullah, S., Schlerf, M., Skidmore, A.K., Hecker, C., 2012. Identifying plant species using mid-wave infrared (2.5–6 μm) and thermal infrared (8–14 μm) emissivity spectra. Remote Sens. Environ. 118, 95–102.
Ullah, S., Skidmore, A.K., Ramoelo, A., Groen, T.A., Naeem, M., Ali, A., 2014. Retrieval of leaf water content spanning the visible to thermal infrared spectra. ISPRS J. Photogramm. Remote Sens. 93, 56–64.
Ustin, S.L., 2013. Remote sensing of canopy chemistry. United States of America]–>Proc. Natl. Acad. Sci. U. S. A. 110 (3), 804–805.
Ustin, S.L., Roberts, D.A., Pinzo, J., Jacquemoud, S., Gardner, M., Scheer, G., Castan, C.M., 1998. Estimating canopy water content of chaparral shrubs using optical methods. Remote Sens. Environ. 65, 280–291.
Westoby, M., 1998. A leaf-height-seed (LHS) plant ecology strategy scheme. Plant Soil 199 (2), 213–227. http://dx.doi.org/10.1023/A:1004327224729.
Wold, S., Sjostrom, M., 2001. PLS-regression: a basic tool of chemometrics. Chemom. Intell. Lab. Syst. 58, 109–130.
Young, S.J., Johnson, R., Hackwell, J.A., 2002. An in-scene method for atmospheric compensation of thermal hyperspectral data. J. Geophys. Res. 107 (D24) (ACH 14–1–ACH 14–20).